博士論文（要約）

Analysis of a novel lipolytic enzyme that links phospholipids to epigenetic regulation

（リン脂質とエピゲノムをつなぐ新規脂質分解酵素の解析）

原田（辻） 小夜可

博士論文

Analysis of a novel lipolytic enzyme that link phospholipids to epigenetic regulation

（リン脂質とエピゲノムをつなぐ新規脂質分解酵素の解析）

The University of Tokyo

Graduate School of Medical Science

Department of Social Medicine

Name　Sayaka (Tsuji) Harada

Supervisor　Professor. Makoto Murakami

Abstract

PNPLA7, a member of the phospholipase A_2 family, acts as a fasting-inducible lysophospholipase that converts lysophosphatidylcholine to glycerophosphocholine, a precursor of endogenous choline. Our recent study using *Pnpla7*-null mice revealed that PNPLA7-driven phospholipid catabolism is linked to hepatic choline/methionine metabolism for the production of S-adenosylmethionine (SAM), a universal methyl donor. The aims of the present study are to examine whether the expression of *PNPLA7* could be nutritionally regulated by certain choline/methionine metabolites, whether the reduced SAM flux in *Pnpla7*-null mice could affect the methylation of histones and DNA, and whether *PNPLA7* expression would be affected in human liver cancer. We found that the expression of *PNPLA7* was induced in human hepatocarcinoma following methionine depletion and downregulated following methionine re-supplementation. Metabolome analysis revealed marked reductions of methionine and SAM as well as many other related metabolites in methionine-depleted cells. The reduction of SAM decreased the methylation of the *PNPLA7* promoter, allowing upregulation of *PNPLA7* expression. In accordance with the decrease in hepatic SAM levels, the methylation levels of several histones and DNA promoters were noticeably reduced in the liver of *Pnpla7*$^{-/-}$ mice relative to *Pnpla7*$^{+/+}$ mice, indicating that the *PNPLA7*-driven SAM pool is coupled with specific histone and DNA methylation events *in vivo*. Furthermore, in line with previous studies that SAM supplementation prevents the growth and invasion of liver cancer,

the expression of *PNPLA7* as well as other methionine cycle enzymes was markedly reduced in human hepatocellular carcinoma. Overall, this study revealed a previously unrecognized association of phospholipid metabolism with epigenetic regulation.

Abbreviation

AHCY, adenosylhomocysteinase

ADP, adenosine diphosphate

AMP, adenosine monophosphate

ATP, adenosine triphosphate

BHMT, betaine homocysteine *S*-methyltransferase

CE-MS, capillary electrophoresis-mass spectrometry

CDP, cytidine diphosphate

CTP, cytidine triphosphate

DHAP, dihydroxyacetone phosphate

DHF, dihydrofolate

dADP, deoxyadenosine diphosphate

dATP, deoxyadenosine triphosphate

dCDP, deoxycytidine diphosphate

dCTP, deoxycytidine triphosphate

dGDP, deoxyguanosine diphosphate

dGTP, deoxyguanosine triphosphate

DNMT, DNA methyltransferase

dUDP, deoxyuridine diphosphate

dUMP, deoxyuridine monophosphate

dTMP, deoxyuridine triphosphate

dTTP, deoxythymidine triphosphate

FBS, fetal bovine serum

FOXO, forkhead box o1

F1,6BP, fructose 1,6-bisphosphate

F1,6P, fructose 1,6-phosphate

F6P, fructose 6-phosphate

GDE, glycerophosphodiesterase

GDP, guanosine diphosphate

GMP, guanosine monophosphate

GNMT, glycine-*N*-methyltransferase

GPC, *sn*-glycero-3-phosphocholine

GSH, glutathione

GSSG, glutathione-S-S-glutathione

GTP, guanosine triphosphate

G3P, glycerol 3-phosphate

G6P, glucose 6-phosphate

HBV, hepatitis B virus

Hcy, homocysteine

HMT, histone methyltransferase

IMP, inosinmonophosphat

iPLA$_2$, Ca^{2+}-independent PLA$_2$

LC-ESI-MS, liquid chromatography-electrospray ionization-tandem mass spectrometry

LPC, lysophosphatidylcholine

LPE, lysophosphatidylethanolamine

MAT1A, methionine adenosyltransferase 1A

MCD, methionine and choline-deficient diet

MRM, multiple reaction monitoring

MSRE-PCR, methylation-sensitive restriction enzymes-polymerase chain reaction

5mCs, 5-methylcytosines

MTA, 5'-methylthioadenosine

MTR, 5-methyltetrahydrofolate-homocysteine methyltransferase

NAD^+, nicotinamide adenine dinucleotide, oxidized

NADH, nicotinamide adenine dinucleotide, reduced

$NADP^+$, nicotinamide adenine dinucleotide phosphate, oxidized

NADPH, nicotinamide adenine dinucleotide phosphate, reduced

NAFLD, nonalcoholic fatty liver disease

NASH, non-alcoholic steatohepatitis

PBS, phosphate-buffered saline

PC, phosphatidylcholine

PE, phosphatidylethanolamine

PEMT, PE *N*-methyltransferase

PEP, phosphoenolpyruvate

PNPLA, patatin-like phospholipase domain containing protein

PRPP, phosphoribosyl pyrophosphate

RRBS, reduced representation bisulfite sequencing

SAH, *S*-adenosyl-L-homocysteine

SAM, *S*-adenosylmethionine

THF, tetrahydrofolate

UDP, uridine diphosphate

UMP, uridine monophosphate

UTP, uridine triphosphate

2,3-DPG, 2,3-diphosphoglycerate

2PG, 2-phosphoglycerate

3PG, 3-phosphoglycerate

Contents

Introduction ……. 1

Materials and Methods ……. 9

Results ……. 20

The expression of PNPLA7 is nutritionally regulated by choline and methionine 21

The expression of PNPLA7 is regulated by methionine availability 22

The expression of PNPLA7 is reversed by re-supplementation of methionine 23

Metabolomic analysis reveals alterations of various metabolites related to methionine metabolism 24

Methionine deficiency decreases the methylation of the PNPLA7 gene promoter 30

The PNPLA7-dependent SAM production is linked to epigenetic regulation by modifying histone and DNA methylation 31

Expression of PNPLA7 and related enzymes in human hepatocellular carcinoma 34

Discussion ……. 60

Conclusion ……. 76

References ……. 78

Acknowledgment ……. 97

Introduction

Choline is recognized as an essential dietary nutrient for normal body function due to its broad range of functions as a precursor of the neurotransmitter acetylcholine, as a structural component of membrane phospholipids, and as a source of methyl group metabolism (Zeisel and da Costa, 2009). Since the amount of choline generated endogenously has long been thought to be insufficient to meet requirements, it needs to be obtained from foods. Choline is an essential element to generate several metabolites in the choline cycle including phosphatidylcholine (PC) and lysophosphatidylcholine (LPC), the former of which is a major cell membrane component. More than 95% of cellular choline exists as PC in cellular membrane, indicating that this phospholipid represents the most abundant reserve pool of total cellular choline. PC can be produced from choline through *de novo* synthesis called the Kennedy pathway, in which choline is converted to phosphocholine by choline kinase, then to CDP-choline by choline cytidylyltransferase, and finally to PC by choline phosphotransferase. Liver has an alternative PC-biosynthetic pathway that constitutes three-step methylation of phosphatidylethanolamine (PE) to generate PC by PE *N*-methyltransferase (PEMT), which accounts for 5–40% of total hepatic PC synthesis and is the only known route for *de novo* biosynthesis of the choline moiety in mammals (Robinson et al., 2016; Vance, 2013). Choline is also oxidized to betaine in some cell types such as hepatocytes, and production of betaine is crucial to synthesize *S*-adenosylmethionine (SAM), which is a universal methyl donor.

Methionine is an essential and sulfur-containing amino acid that is involved in various biological responses such as DNA and histone methylation for epigenetic regulation of gene expression, redox maintenance, polyamine generation, and protein synthesis, and is also directly associated with folate metabolism (Sanderson et al., 2019). In the methionine cycle, homocysteine (Hcy), a precursor of methionine, is remethylated back to methionine by either methionine synthase (MTR), which transfers a methyl group from 5-methyl tetrahydrofolate (THF) in the folate cycle in concert with vitamin B_{12}, or betaine homocysteine S-methyltransferase (BHMT), which transfers a methyl group from betaine (Abbasi et al., 2017; Kempson et al., 2014; Li et al., 1996). Considering that betaine is an oxidized product of choline ($(CH_3)_3N^+CH_2CH_2OH \rightarrow (CH_3)_3N^+CH_2COOH$) (Delgado-Reyes et al., 2001), both choline and methionine are interconnected via BHMT. Dietary methionine is partitioned and, when not incorporated into proteins, is adenylated to form SAM by methionine adenosyltransferase 1A (MAT1A). SAM is required for numerous transmethylation reactions for nucleic acids, proteins, lipids, and small molecules (McBreairty and Bertolo, 2016). In mammals, ~50% of methionine metabolism and ~85% of transmethylation take place in the liver. SAM is converted to S-adenosylhomocysteine (SAH) as a byproduct of transmethylation reactions. SAH is hydrolyzed by SAH hydrolase (AHCY) to adenosine and homocysteine, the latter of which is then converted back to methionine by receiving a methyl group from 5-methyl-THF/vitamin B_{12} via the folate cycle or from betaine via the choline cycle.

Intracellular levels of SAM vary depending on cellular nutrient conditions and affect the activity of histone methyltransferases (HMT), linking cellular nutrient metabolism and histone methylation (Mentch and Locasale, 2016). Histone methylation is crucial for the regulation of chromatin remodeling and gene transcription (Mentch and Locasale, 2016). Several studies have reported that the expression of MAT1A, an enzyme that synthesizes SAM, is correlated with the induction of histone H3K27 trimethylation in the liver, an epigenetic modification that leads to gene silencing (Ramani and Lu, 2017; Reytor et al., 2009). SAM levels also affect the methylation of genomic DNA by DNA methyltransferases (DNMTs). Methylation of CpG islands by DNMTs is an important component of the epigenetic code and a number of genes become abnormally methylated during tumorigenesis (Gujar et al., 2019; Li and Tollefsbol, 2010). Furthermore, as mentioned above, three methyl groups in SAM are transferred to PE, resulting in the generation of one molecule of PC, by PEMT in the liver. The schematic outline of this research is illustrated in Figure 1.

The importance of choline and methionine metabolism has been gained mostly from genetic or dietary models that harbor chronic choline/methyl group deficiency or excess in rodents. Mice fed a methionine/choline-deficient diet exhibit various abnormalities including decreased PC synthesis, inadequate supply of labile methyl groups, and adaptive changes in lipid metabolism (da Costa et al., 2004; da Costa et al., 2006). These metabolic alterations can cause hepatic steatosis, impaired lipoprotein secretion, hypoglycemia, hypermetabolism,

muscle weakness, growth retardation, and reduced adiposity. Moreover, genetic deletion of BHMT, a rate-limiting enzyme for the methyl group flux from choline to methionine, recapitulates several of these phenotypes (Teng et al., 2012).

PC is hydrolyzed by phospholipase A_2 (PLA_2) or PLA_1 enzymes to fatty acid and LPC (Bjorkoy et al., 1995; Larrodera et al., 1990; Martin et al., 1997). Mammalian genome encodes more than 50 PLA_2s or related enzymes, which are classified into several subfamilies on the basis of their structures and functions (Murakami, 2017; Murakami et al., 2011). In a general view, the PLA_2 family has mainly been implicated in signal transduction by producing lipid mediators derived from lysophospholipid or polyunsaturated fatty acids. LPC is converted back to PC by lysophospholipid acyltransferases, a pathway known as the Lands' cycle (Harayama et al., 2014; Shindou and Shimizu, 2009). Additionally, LPC is further hydrolyzed by lysophospholipase to give rise to glycerophosphocholine (GPC), which is further catabolized to choline and glycerol-3-phosphate by glycerophosphodiesterases (GDEs) (Yanaka, 2007). However, the PC-catabolic pathway (PC $\rightarrow$ LPC $\rightarrow$ GPC $\rightarrow$ choline) has currently received much less attention, and accordingly, molecular entities of the enzymes responsible for the PC catabolism and its biological importance remained to be largely obscure.

In an effort to clarify the biological roles of PLA_2s and related enzymes by gene targeting (Murakami, 2017), our research group has recently found that two enzymes in the patatin-like PLA_2 (PNPLA; also known as Ca^{2+}-independent PLA_2 ($iPLA_2$)) family (Figure 2),

PNPLA7 (a fasting-inducible lysophospholipase) and PNPLA8 (a PLA_2 that lies upstream of PNPLA7), are responsible for hepatic PC catabolism to regulate the release of water-soluble choline from hydrophobic PC, allowing mobilization of methyl groups to the methionine cycle. Genetic ablation of either PNPLA7 or PNPLA8 markedly impairs hepatic PC catabolism, leading to the phenotypes reminiscent of methionine insufficiency (Hirabayashi et al, manuscript in preparation). These results strongly suggest that the continuous methyl group flux through the PNPLA8/7-driven PC-catabolic pathway plays an important role in hepatic functions and systemic energy homeostasis.

However, several points still remained to be unsolved. Accordingly, the aims of the present study are to examine 1) whether the expression of PNPLA7 could be nutritionally regulated by certain choline/methionine metabolites in cultured cells, 2) whether the reduced flux of SAM as a result of *PNPLA7* deficiency could affect the methylation status of histones and genomes DNA in mice, and 3) whether the expression of *PNPLA7* and/or related enzymes would be affected in human liver disease.

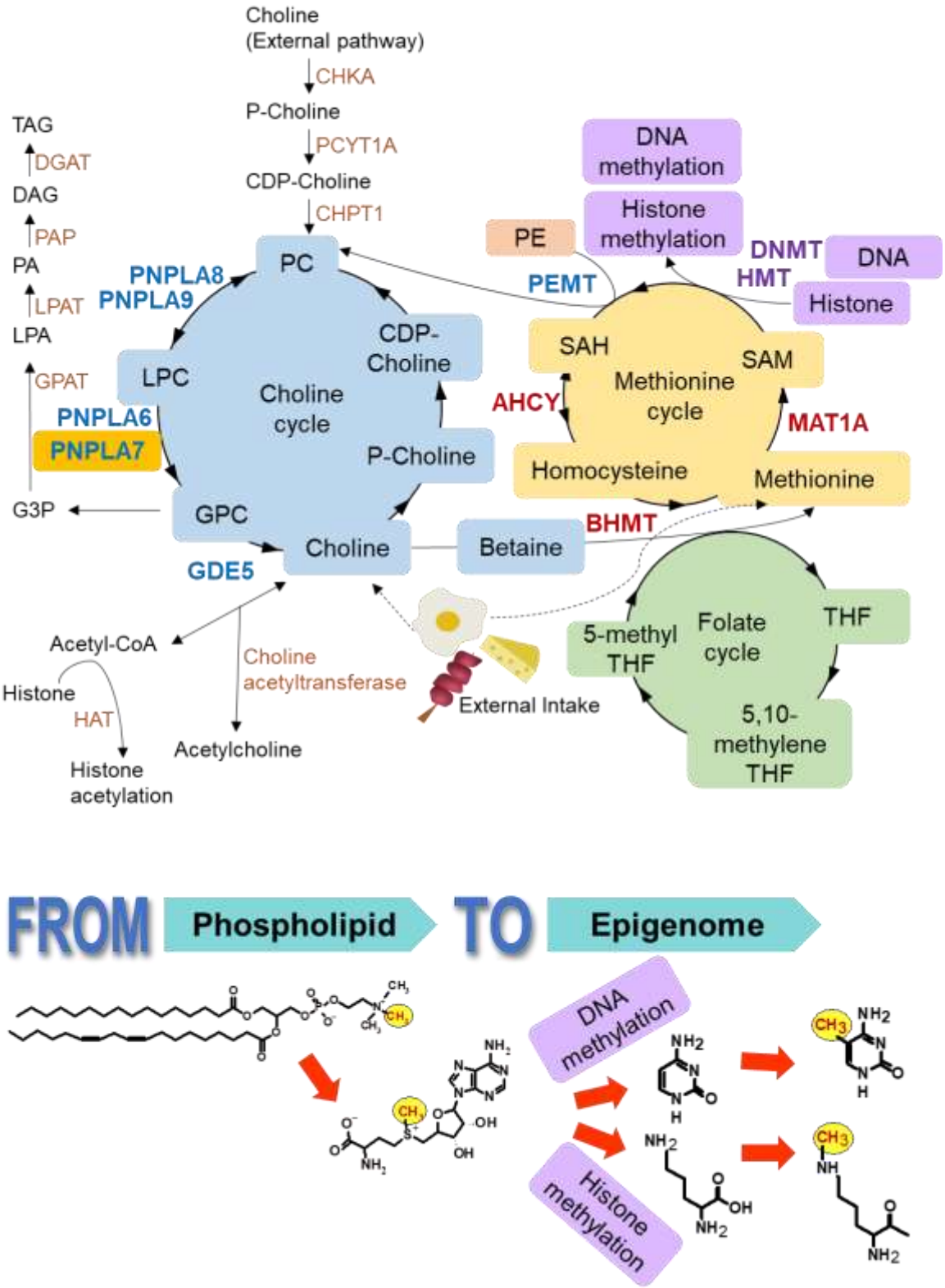

Figure 1. Schematic outline of the research. (a) Overview of the metabolic map associated with choline and methionine metabolism. The main metabolites and enzymes involved in this metabolic pathway are indicated. Abbreviations of representative metabolites and enzymes are described in the main text. (b) A putative methyl group flux from phospholipid to DNA and histone methylation through SAM, which is one of the main issues to be clarified in this study.

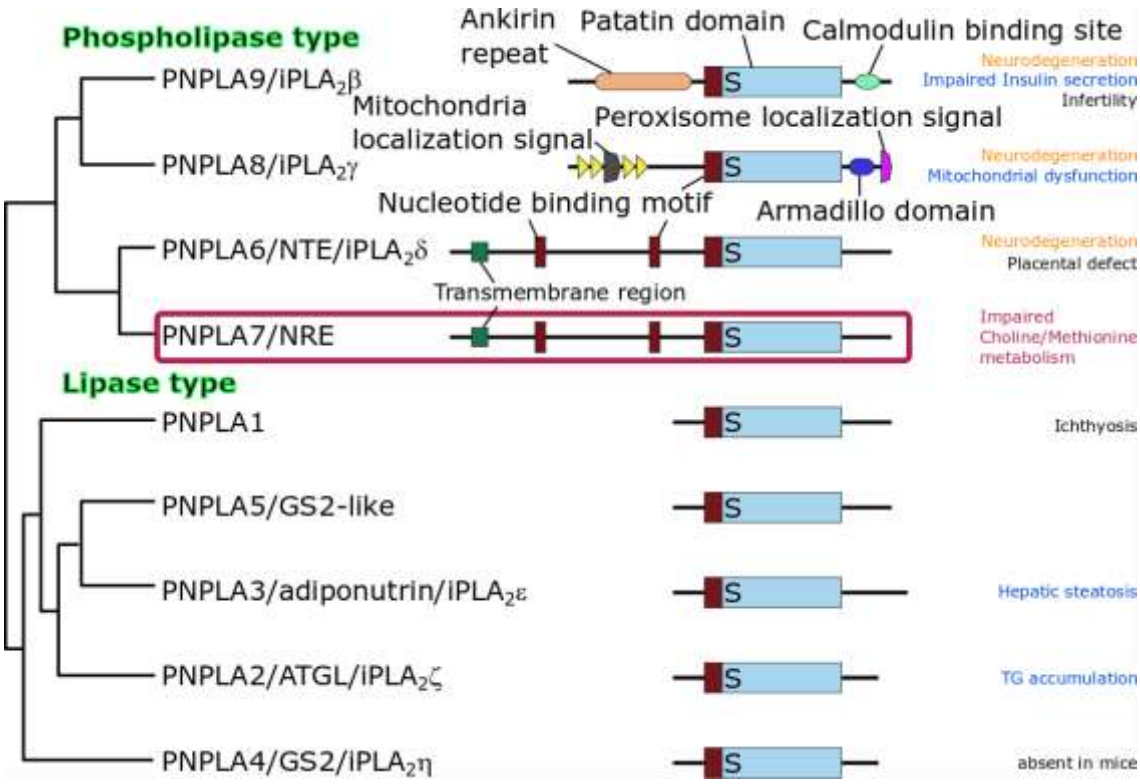

Figure 2. Names, structures, *in vivo* functions, and enzymatic activities of the PNPLA/iPLA$_2$ family. This family contains 9 isoforms, all of which have a conserved patatin domain. PNPLA6-9 act on phospholipids (phospholipase type), while PNPLA1-5 act on neutral lipids (lipase type). Mutations or deletion of these enzymes leads to metabolic dysfunction (blue), neurodegeneration (orange), and others. This study focuses on PNPLA7, whose genetic deletion leads to impaired choline and methionine metabolism in the liver.

Materials and Methods

Cell culture

The human hepatocarcinoma cell line used in this study, HepG2 (JCRB Cell Bank, JCRB1054), was cultured in Dulbecco's Modified Eagle's Medium (D-MEM/Ham's F-12 with L-Glutamine and Phenol Red, Fujifilm Wako Pure Chemical, #048-29785) supplemented with 10% (v/v) heat-inactivated fetal bovine serum (FBS; Thermo Fischer Scientific, lot No. 42Q5084K, #10270-106) and 1% (w/v) penicillin-streptomycin (Thermo Fischer Scientific, #15140122). Cell cultures were maintained at 37℃ in a 95% humidified incubator containing 5% CO_2. For methionine and/or choline starvation experiments, the cells were cultured in 10% FBS medium on polystyrene-coated 24-well culture plates (IWAKI) at a density of 5×10^4 cells/mL for 24 hours. Cells were washed twice with 500 μL of phosphate-buffered saline (PBS) and replenished with the methionine and/or choline restriction medium with or without addition of methionine and/or choline for different exposure times (24, 48, 72, and 96 hours). At the end of each culture condition, the medium was removed and washed with 500 μL of PBS twice.

Cell proliferation assay

Cell proliferation was determined by cell counting and MTT assay (Vybrant MTT Cell Proliferation Assay Kit, Thermo Fischer Scientific, #V-13154). For cell counting, cells were stained with trypan blue after trypsinization and counted under the microscope using

hemocytometer. For the MTT assay, cells were cultured in 10% FBS medium on polystyrene-coated 96-well culture plates (IWAKI) at a density of 500 cells/μL for 24 hours. Cells were washed twice with 100 μL of PBS and replenished with 80 μL of methionine restriction medium with or without addition of methionine for 48 hours. The remaining procedures were according to the manufacturer's instructions. The absorbance at 560 nm for 0.1 second was read using a plate reader (Wallac 1420 ARVO MX, Perkin Elmer).

Metabolomic analysis

Metabolomic analysis was done in collaboration with Dr. Soga (Keio University, Tsuruoka) using capillary electrophoresis-mass spectrometry (CE-MS) (Satoh et al., 2017). HepG2 cells were cultured in 10% FBS medium on collagen-coated 100 mm culture dish (IWAKI) at a density of 5×10^4 cells/mL for 48 hours. After aspirating the medium, the cells were washed twice with 10 mL of 5% mannitol and leave at rest for 10 minutes at room temperature in 1 mL of methanol containing 25 μM L-methionine sulfone (Fujifilm Wako Pure Chemical, #502-76641), 25 μM 2-(*N*-morpholino) ethanesulfonic acid (MES; Dojindo, #349-01623), and 25 μM *D*-camphor-10-sulfonic acid (CSA; Fujifilm Wako Pure Chemical, #037-01032). The cells were harvested with a cell scraper and 400 μL of the supernatant was collected after vortexing for 30 seconds. After adding 400 μL of $CHCl_3$ and 200 μL of distilled water with thorough mixing, centrifugation was performed at 10,000g for 3 minutes at 4℃. Then 400

μL of the aqueous layer were transferred to an HMT 5 kDa ultrafiltration tube (Ultrafree-MC-PLHCC 250/pk, Human Metabolome Technologies, UFC3LCCNB-HMT). This was followed by centrifugation at 9,100g for 2 hours at 20℃. The collection through the filtration was shipped to the Institute for Advanced Biosciences at Keio University for further analysis.

Lipidomics

Lipid metabolome analysis was performed using liquid chromatography-electrospray ionization mass spectrometry (LC-ESI-MS). Lipids were extracted from HepG2 cells using the method of Bligh and Dyer (Bligh and Dyer, 1959). Phospholipids in lipid extracts were quantitated by the inorganic phosphorus assay (Lee et al., 2012). Internal standards for each lipid (PC 25:0, #LM1000-1EA; PE 25:0, #LM1100-1EA; LPC 16:0-d49, #870308; Avanti Polar Lipids) were added to the samples before LC-ESI-MS/MS analysis. The LC-ESI-MS/MS analysis was performed on a Shimadzu Nexera ultra high-performance liquid chromatography (UHPLC) system (Shimadzu) coupled with a QTRAP 4500 hybrid triple quadrupole linear ion trap mass spectrometer (AB SCIEX). Chromatographic separation was performed on an ZIC-HILIC column (250 mm x 2.1 mm, 3.5 μm; Waters) maintained at 40°C using mobile phase A [acetonitrile/water (50/50, v/v) containing 20 mM ammonium acetate] and mobile phase B [acetonitrile/water (95/5, v/v) containing 10 mM ammonium acetate] in a gradient program (0−11 min: 0% B→52% B; 11−15 min: 52% B→90% B; 15−15.5 min: 90% B; 15.51−20 min: 0%

B), with a flow rate of 0.3 ml/min. Lipids were analyzed by Multiple Reaction Monitoring (MRM) in the positive ion mode. Neutral loss scans of 74 Da were used to detect PC molecular species. Precursor ion scan of m/z = 196 was used to detect PE molecular species. Mass spectrometer conditions are as follows: curtain gas, 10 psi; collision gas, 7 arbitrary units; ionspray voltage, 4500 V; source temperature, 700°C; ion source gas 1, 30 psi; ion source gas 2, 50 psi; declustering potential, 171 V (for PC) or 116 V (for PE); entrance potential, 10 V; collision energy, 37 V (for PC) or 31 V (for PE); and collision cell exit potential, 14 V (for PC) or 12 V (for PE). MRM data were analyzed by MultiQuant and Analyst software (AB SCIEX). Quantification was performed by integration of the peak area of the extracted ion chromatograms for each lipid.

Reverse transcription (RT)-quantitative PCR (qPCR)

Total RNA was extracted from tissues and cells using the TRIzol Reagent (Thermo Fischer Scientific, #15596018). cDNA was synthesized from 2 μg of total RNA using random primers and a High-Capacity cDNA Reverse-Transcription Kit (Thermo Fischer Scientific, #4368813). PCRs were carried out using TaqMan Gene Expression Master Mix (Thermo Fischer Scientific, #4369016) and TaqMan Gene Expression Assays (TaqMan probe-primer sets) on a StepOnePlus Real-Time PCR System (Thermo Fischer Scientific). The probe-primer sets are listed in Table 1. Gene expression data were corrected against *GAPDH* (mouse, 4352339E;

human, 4326317E, Thermo Fischer Scientific) control gene expression and normalized using the $\Delta\Delta C_T$ method.

Pnpla7-deficient mice

Pnpla7 floxed mice (Hirabayashi et al, manuscript in preparation) were bred with *CAG-Cre* mice (RBRC01828) (Matsumura et al., 2004) to generate global heterozygous knockout mice (*Pnpla7*$^{+/-}$). The male and female heterozygous mice were intercrossed to obtain homozygous null mice (*Pnpla7*$^{-/-}$), and littermate WT mice (*Pnpla7*$^{+/+}$) were used as controls. Mice were fed ad libitum a hydrated diet (DietGel76A, ClearH_2O), had free access to water, and were kept on a 12:12-hour light:dark cycle at 23℃. All experimental procedures involving animals were approved by the Institutional Animal Care and Use Committees of Tokyo Metropolitan Institute of Medical Science and the University of Tokyo, and were conducted in accordance with the Japanese Guide for the Care and Use of Laboratory Animals.

Microarray analysis

The quality of RNA was verified with a 2100 Bioanalyzer (Agilent Technologies). Fluorescently labelled antisense RNA (cDNA target) was synthesized with a Low Input QuickAmp Labelling Kit (Agilent Technologies) according to the manufacture's protocol. Samples were hybridized to the Mouse Gene Expression 4 x 44 K v2 Microarray (G4846A,

Agilent Technologies), washed, and then scanned using a SureScan Microarray Scanner (Agilent Technologies). Microarray data were analyzed with Feature Extraction software (Agilent Technologies) and then imported into GeneSpring GX software (Agilent Technologies). Signal intensities were normalized by global normalization.

Methylation analysis

Pnpla7$^{+/+}$ and *Pnpla7*$^{-/-}$ mice (6-week-old, male) were anesthetized and perfused intracardially with saline containing 1 mM MOPS, pH 7.4. Freshly isolated livers were frozen immediately in liquid nitrogen and stored at -80℃. The frozen livers were shipped to Active Motif Inc. for analysis of histone methylation (https://www.activemotif.jp/catalog/1235/mod-spec, https://www.activemotif.jp/ documents/2077.pdf (Zheng et al., 2013) and DNA methylation (https://www.activemotif.jp/documents/1836.pdf). Extractions of histones and DNA from mouse livers, and analyses of them were carried out using mass spectrometry for histone methylation and reduced representation bisulfite sequencing (RRBS) for DNA methylation according to manufacturer's instructions, respectively. Histones were acid-extracted from cell pellets and trypsinized to digest them. Trypsin-digested histones were analyzed and quantified by first calculating the sum of peak areas of corresponding peptide transitions, then the total pool of modifications for that residue was calculated on the sum of all modified forms for each amino acid. Each modification is then shown as a percentage of the

total pool of modifications. The hierarchical clustering heatmap was developed using default setting of pheatmap function in R (version 3.3.3). RRBS analysis provides a method to quantify methylation levels for unique CpG sites in the promoter 2K region (0 to 2,000 bp upstream of the transcriptional start site). The steps of RRBS analysis involved DNA digestion using the restriction enzyme *Msp*I, which cuts DNA at its recognition site, CCGG, independently of the CpG methylation status. Subsequent reactions of DNA end repair, A-tailing and adaptor ligation were followed by Illumina sequencing (NextSeq 500) after size selection. Then bisulfite conversion was performed for total genomic DNA. Bisulfite conversion with sodium bisulfite allows conversion of cytosines to uracils in a single stranded DNA, whereas 5-methylcytosines (5mCs) are resistant to this conversion and remain as cytosines, allowing 5mCs to be distinguished from unmethylated cytosines. During a subsequent PCR amplification, the DNA sequences are amplified with primers specific for one strand of uracil converted from methylated cytosine, and uracil is amplified as thymine. If cytosine in the CpG dinucleotide exists as 5mC, PCR recognizes 5mC as cytosine (Bock et al., 2010; Bonora et al., 2019; Harris et al., 2010) (see Figure 10b, c).

Methylation-sensitive restriction enzyme-dependent PCR (MSRE-PCR)

Genomic DNA was isolated by cell lysis with 465 μL of digestion buffer A (50 mM Tris-HCl, pH 8.0; 1 mM EDTA) and 25 μL of digestion buffer B (0.6% SDS), and 400 μg/mL

proteinase K (P6556, Sigma-Aldrich) thorough mixing. After incubation for overnight at 55℃, DNA was extracted with phenol and chloroform and precipitated with ethanol. This was followed by centrifugation at 15,000 rpm for 10 minutes at 4℃. The pellets were washed with 70% ethanol, centrifuged at 15,000 rpm for 5 minutes at 4℃, and resuspended in TE buffer (10 mM Tris-HCl, pH 8.0; 1 mmol/L EDTA, pH 8.0).

MSRE-PCR was performed in accordance with previous studies (Aiba et al., 2019; Aiba et al., 2017) with modifications. Briefly, purified genomic DNA was digested with the methylation-sensitive restriction enzyme *Eag*I. The resulting digested DNA samples were subjected to relative quantitative PCR measurements by a LightCycler (Roche Diagnostics GmbH) with a forward primer 5'-GGTTCGTGCAGATCAAGGAG-3' and a reverse primer 5'-GTTGTCAGGGTCGAAGGTACC-3'. The ratio of target DNA amounts was determined using the ΔΔCt method in which the PCR efficiency is considered 2 and the methylation levels (expressed as % methylation) of *Eag*I-CpG sites were calculated relative to those of untreated DNA, whose methylation level was set at 100%.

Clinical samples

The liver samples analyzed in the present study were obtained from the patients who had been treated in the Hepatobiliary Pancreatic Division, Department of Surgery, the University of Tokyo Hospital (Enooku et al., 2016). All the enrolled patients underwent liver resection for

the treatment of hepatocellular carcinoma. RNA (2 μg) extracted from the enrolled patients was reverse transcribed to cDNA. RT-qPCR were done according to the manufacturer's protocol using the TaqMan Gene Expression Assay for *PNPLA6-9* and major metabolic enzymes in choline/methionine cycle (Table 1). This study was carried out in accordance with the ethical guidelines of the 1975 Declaration of Helsinki and was approved by the Institutional Research Ethics Committee of the University of Tokyo. A written informed consent was obtained for the use of the samples.

Statistical analysis

All measurements were performed in duplicate, triplicate or more according to the experiments. No data were excluded from the analysis. Data are presented as mean ± standard error of the mean (SEM) or mean ± standard deviation (SD). Comparison of two groups of data were analyzed by the Student's paired two-tailed *t* test, while multiple-group data were analyzed with one-way ANOVA with Turkey's multiple comparison test (*post hoc*) for *in vitro* experiments. A paired t test in GraphPad Prism was used for clinical study using hepatocellular carcinoma (tumor) and the matched non-hepatocellular carcinoma (non-tumor) samples. The significance was indicated as follows: †, $P < 0.05$; ††, $P < 0.01$.

Table 1. A list of probe/primer sets for real-time PCR. (a) Mouse (b) Human

(a)

Gene name	Assay ID	Gene name	Assay ID
Pnpla6	Mm00450144_m1	*Pnpla8*	Mm00470656_m1
Pnpla7	Mm00461560_m1	*Pnpla9*	Mm01299492_m1

(b)

Gene name	Assay ID	Gene name	Assay ID
PLA2G1B	Hs00386701_m1	*PLA2G4E*	Hs00416278_m1
PLA2G2A	Hs00179898_m1	*PLA2G4F*	Hs02577398_m1
PLA2G2D	Hs01572940_m1	*PNPLA6*	Hs00210447_m1
PLA2G2E	Hs01573049_g1	*PNPLA7*	Hs00173472_m1
PLA2G2F	Hs00224482_m1	*PNPLA8*	Hs00358567_m1
PLA2G3	Hs00210447_m1	*PNPLA9*	Hs00913513_m1
PLA2G5	Hs00173472_m1	*AHCY*	Hs00426322_m1
PLA2G10	Hs00358567_m1	*BHMT*	Hs01566156_m1
PLA2G12A	Hs00913513_m1	*GPCPD1*	Hs00325631_m1
PLA2G4A	Hs00996915_m1	*MAT1A*	Hs01547962_m1
PLA2G4B	Hs00979965_m1	*PEMT*	Hs01002999_m1
PLA2G4D	Hs00603557_m1		

Results

The expression of PNPLA7 is nutritionally regulated by choline and methionine

Our previous study showed that *Pnpla7* was upregulated in the liver and adipose tissue of mice with fasting for 24 hours, implying that the expression of *Pnpla7* is regulated by nutritionally-controlled status in the liver. However, it remained unknown as to which nutritional components could influence the expression of this enzyme. Feeding a diet deficient in both methionine and choline (MCD) is the most widespread method to study non-alcoholic steatohepatitis (NASH). Mice fed a MCD diet (da Costa et al., 2004; da Costa et al., 2006), or those disrupted for *Bhmt, Mat1a* and *Pemt,* which are involved in choline and methionine metabolism (Cano et al., 2011; Li et al., 2006; Teng et al., 2012), exhibit various abnormalities including decreased PC synthesis, perturbed methyl group supply, and adaptive changes in hepatic and systemic metabolism. Since PNPLA7 is considered to be functionally linked to choline and methionine metabolism, we hypothesized that its expression would be regulated by some metabolites in this metabolic pathway.

To assess whether the expression of PNPLA7 (or any other PLA_2 subtypes) would be affected by restriction of some nutrients (such as methionine and/or choline) even in cultured cells, we used a human hepatocarcinoma HepG2 cell line that was cultured in medium supplemented with or without methionine and choline (Figure 3(a)). The morphology of the cells was not altered even after culture for 48 hours in the absence of methionine and choline (Figure 3(b)). Deficiency of methionine, rather than choline, has been reported to suppress cell

growth (Wang et al., 2019). Indeed, proliferation of HepG2 cells cultured in medium without both methionine and choline (Figure 3(c)) or without methionine alone, as assessed by cell counting (Figure 3(d)) and MTT assay (Figure 3(e)), was not altered by 24 hours but was significantly reduced at 48 hours in comparison with the cells cultured in normal medium, confirming that the lack of methionine supplementation prevents cell proliferation.

We performed quantitative real-time PCR to explore the overall effects on the gene expression of various PLA_2 enzymes in this context (Figure 3(f)). The results revealed that the expression of *PLA2G12A* and *PNPLA7* were significantly upregulated, whereas that of *PLA2G1B* and *PLA2G3* were significantly downregulated, in cells cultured without both methionine and choline for 48 hours. The expression of *PNPLA8* and *PNPLA9*, two other members of the PNPLA family, also tended to be increased in culture without methionine and choline, although this difference did not reach statistical significance. Focusing on PNPLA7, these results indicate that *PNPLA7* is upregulated under the influence of methionine and/or choline depletion *in vitro* (and also probably *in vivo*, based on its upregulation during fasting).

The expression of *PNPLA7* is regulated by methionine availability

A dietary methionine restriction is considered to decrease *de novo* lipogenesis and increase lipolysis and fatty acid oxidation by downregulating lipogenic genes and upregulating lipolytic and β-oxidation genes (Castellano et al., 2015; Hasek et al., 2013; Zhou et al., 2016). These

previous studies have raised the possibility that methionine depletion might be sufficient to upregulate the expression of PNPLA7. To examine the hypothesis, we used four kinds of media with different compositions, which were normal (= methionine/choline-sufficient), choline-deficient, methionine-deficient, and both methionine- and choline-deficient, on which HepG2 cells could have wide scope for their metabolic processes. Using quantitative real-time PCR, we examined the expression levels of *PNPLA6-9* (Figure 4(a)) and several other enzymes related to choline and methionine metabolism (Figure 4(b)). Notably, *PNPLA7* was markedly upregulated in HepG2 cells cultured in methionine-depleted or methionine/choline-depleted medium, but not choline-depleted medium, over 24-72 hours (Figure 4(a)). In comparison, *PNPLA6, PNPLA8* and *PNPLA9* were increased only modestly under these culture conditions (Figure 4(a)). Genes related to the choline and methionine cycles were barely affected (*GDE5, MAT1A* and *AHCY*) or decreased (*BHMT*) by methionine and/or choline depletion (Figure 4(b)). Altogether, among the enzymes involved in the choline and methionine metabolism, *PNPLA7* is the most dramatically upregulated gene in response to methionine depletion.

The expression of PNPLA7 is reversed by re-supplementation of methionine

If methionine restriction is a crucial condition to boost *PNPLA7* expression, re-supplementation of methionine might reduce its expression. To confirm this hypothesis, we performed the reverse experiment, in which HepG2 cells were initially cultured in the absence

of methionine for 72 hours and then re-supplemented with methionine (Figure 5(a)). In the absence of methionine, *PNPLA7* was highly upregulated in HepG2 cells, as described above. Continuous culture of these cells with medium re-supplemented with methionine over 48-72 hours (at 120, and 144 hours, respectively, in Figure 5(a)) resulted in downregulation of *PNPLA7* depending on duration of the methionine exposure, eventually reducing its expression to a level nearly comparable to that in the cells cultured in normal medium at 144 hours (Figure 5(b)). Likewise, the expression levels of *PNPLA6, PNPLA8* and *PNPLA9*, which had been modestly upregulated in the absence of methionine, were reduced to their normal expression levels after methionine re-supplementation (Figure 5(b)). Altogether, methionine insufficiency is likely the cause of the upregulation of *PNPLA7*.

Metabolomic analysis reveals alterations of various metabolites related to methionine metabolism

To address how methionine deficiency would impact on cellular metabolism, we conducted global metabolome analysis of hydrophilic metabolites and hydrophobic lipids by CE-MS and ESI-MS/MS, respectively. An overview of the metabolic pathways related to methionine metabolism is summarized in Figure 6(a). The effect of methionine deficiency on HepG2 cells was confirmed by the cellular methionine level as it was dramatically reduced (Figure 6(b)). Accordingly, SAM and SAH, which are likely affected by the amount of

methionine in cells, were also markedly reduced. Cystathionine, which links homocysteine in the methionine cycle to the transsulfuration pathway (Zhu et al., 2019), was also decreased to the same degree as methionine, SAM and SAH (Figure 6(b)). Cysteine, which is generated from cystathionine, also showed a decreasing trend in methionine-depleted cells (Figure 6(b)). However, downstream metabolites in the transsulfuration pathway, such as taurine and hipotaurine as well as the reduced and oxidized forms of glutathione (GSH), were barely affected by methionine depletion (Figure 6(b)), suggesting the presence of some bypassing pathways that fuel these metabolites. Interestingly, serine was significantly reduced, while glycine was significantly elevated, in methionine-depleted cells. Since the conversion of serine to glycine is coupled with the folate cycle, the changes in these amino acids may indicate that the transfer of a one-carbon unit from serine was facilitated to maintain the synthesis of 5, 10-methylene-THF and then 5-methyl THF in the folate cycle, which also contribute to supplying the methyl group to regenerate methionine in the presence of vitamin B_{12} (Ducker and Rabinowitz, 2017; Zheng and Cantley, 2019). Moreover, sarcosine, which is generated by direct transfer of a methyl group from SAM to glycine by glycine-*N*-methyltransferase (GNMT) (Luka et al., 2009; Sreekumar et al., 2009), was markedly reduced in methionine-deficient cells, consistent with the fact that SAM as a methyl donor was almost completely depleted (Figure 6(b)).

The amount of 5'-methylthioadenosine (MTA), one of the derivatives from SAM in the methionine salvage pathway, was also markedly reduced in methionine-deficient cells (Figure 6(c)). MTA generation in the methionine salvage pathway is coupled with polyamine biosynthesis (Sauter et al., 2013). Indeed, the amounts of polyamines such as putrescine and spermidine were markedly elevated, while that of spermine was decreased, in methionine-deprived cells (Figure 6(c)), implying that the reduced metabolic flux from SAM to MTA eventually perturbed the polyamine flux, leading to an unusual accumulation of the precursor polyamines (putrescine and spermidine) and a reduction of the polyamine end-product (spermine). These results may accord with a role of polyamines in cell proliferation and anti-aging (Eisenberg et al., 2016; Zabala-Letona et al., 2017) and a role of MTA as an inhibitor of polyamine biosynthesis (Banco et al., 2018). Putrescine is synthesized from ornithine, a metabolite utilized in the urea cycle. In correlation with the increase of precursor polyamines, several metabolites in the urea cycle, including citrulline, urea, argininosuccinate and fumarate, were significantly elevated in methionine-depleted cells (Figure 6(c)).

SAM transfers its methyl group to PE to give rise to PC, a reaction catalyzed by PEMT (Vance, 2013), thus being coupled with the choline cycle. Interestingly, several metabolites in the choline cycle such as GPC, choline, phosphorylcholine, and CDP-choline were increased in methionine-depleted cells (Figure 6(d)), suggesting that the choline cycle, involving catabolism and *de novo* synthesis (Kennedy pathway) of PC, appeared to be activated, in

accordance with the compensatory upregulation of PNPLA7 under the methionine-insufficient condition (Figures 3–5). These results *in vitro* are consistent with those *in vivo*, which showed the decreases of these choline metabolites in *Pnpla7*$^{-/-}$ mice relative to *Pnpla7*$^{+/+}$ mice (see Introduction). Betaine was conversely decreased in methionine-depleted cells (Figure 6(d)), likely because choline might be preferentially fluxed into the Kennedy pathway for *de novo* PC biosynthesis in this context. In addition, the influence of methionine deficiency extended to the ethanolamine cycle, as phosphorylethanolamine and diethanolamine were concomitantly increased upon methionine deprivation (Figure 6(d)). Unexpectedly, despite the reduced SAM flux and thereby reduced PEMT-dependent PC synthesis, PC and its $PLA_{1/2}$-hydrolytic metabolite LPC were largely unchanged, but rather slightly increased (particularly those with polyunsaturated fatty acids), in methionine-deficient cells (Figure 6(e)), implying that the biosynthesis of PC were complemented through another PC-biosynthetic pathway, *i.e.* the Kennedy pathway. Most PE molecular species did not differ significantly between methionine-sufficient and -deficient cells, except that PE34:1 and 34:2 tended to be lower in the absence of methionine (Fig. 6e). These results are consistent with the observations that when the production of PC through PE methylation by SAM is limited, the Kennedy pathway is activated in a complementary fashion to replenish PC, that the Kennedy pathway favors the biosynthesis of PC molecular species with polyunsaturated fatty acids, and that an impairment of the PEMT pathway leads to upregulation of PC catabolism and choline recycling (Li et al., 2005; Li and

Vance, 2008; van der Veen et al., 2017; Vance, 2013). Moreover, the increased ethanolamine metabolites in methionine-depleted cells may indicate that the upregulated PNPLA7 hydrolyzes not only LPC to produce GPC and then choline, but also LPE to produce ethanolamine metabolites. In fact, recombinant PNPLA7 can hydrolyze LPC and LPE as well as lysophosphatidylserine *in vitro* (Heier et al., 2017).

Methionine deficiency also markedly reduced the levels of phosphoribosyl pyrophosphate (PRPP), inosine monophosphate (IMP) and carbamoyl aspartate, suggesting an impairment of *de novo* nucleotide biosynthesis (Figure 6(f)). This could account, at least in part, for cell growth arrest following methionine withdrawal (Figure 3(c)(d)(e)). Despite this, individual nucleotides, probably being replenished by the salvage pathway or other metabolic pathways, were still present and variably affected by methionine deficiency (Figure 6(f)). The levels of ATP, ADP and AMP, reflecting the energy state of the cells, were not significantly affected regardless of methionine availability in this experimental setting. Of note, dTTP was markedly reduced in methionine-depleted cells (Figure 6(f)), which is likely associated with the perturbed supply of a methyl group from the folate cycle that is coupled with the methionine cycle (Gao et al., 2019).

We also investigated glucose metabolism through glycolysis (Figure 6(g)) and TCA cycle (Figure 6(h)) to further understand the metabolic connection with the methionine cycle. Although the amounts of glucose 6-phosphate (G6P), fructose 6-phosphate (F6P), and fructose

1,6-bisphosphate (F1,6BP) were unaffected, downstream metabolites such as dihydroxyacetone phosphate (DHAP), glyceraldehyde 3-phosphate, phosphoenol pyruvate and pyruvate were significantly increased under the methionine-free condition (Figure 6(g)). Given that DHAP can be generated from glycerol 3-phosphate (G3P), a downstream metabolite of GPC that was elevated in methionine-deficient cells (Figure 6(g)), the upregulation of PNPLA7 in response to methionine depletion might contribute to the increased flux from GPC to G3P and then to DHAP for glycolysis. In agreement with the increased glycolytic metabolites, major metabolites in the TCA cycle, such as succinate, fumarate, malate, citrate, cis-aconitate, and isocitrate, were significantly increased in methionine-deficient cells (Figure 6(h)). An overall increase in the TCA cycle metabolites, in association with a decrease in lactate, suggests that methionine depletion increased aerobic respiration. Metabolites in the pentose phosphate pathway, which provides ribose and NADPH, were unchanged regardless of methionine availability (data not shown). Lastly, although acetyl-CoA and malonyl-CoA were below the detection limit in this analysis, the increased NADPH/$NADP^+$ ratio, as revealed by a slight increase in NADPH and a marked reduction of $NADP^+$ after methionine depletion (Figure 6(h)), might reflect that the metabolic flux of *de novo* lipogenesis, which depends on NADPH, is disturbed in methionine-depleted cells, since dietary methionine restriction (Ables et al., 2016) or *Pnpla7* deficiency *in vivo* (see Introduction) also reduces lipogenesis.

Methionine deficiency decreases the methylation of the *PNPLA7* gene promoter

It has been reported that the promoter region of the *PNPLA7* gene is hypermethylated in several human hepatocellular carcinoma cell lines, including HepG2 and Huh7 cells (Figure 7(a)) (Zhang et al., 2016). Accordingly, we speculated that the marked reduction of cellular SAM levels following methionine withdrawal (Figure 6(b)) might decrease the methylation status of the *PNPLA7* promoter, thus allowing the upregulation of *PNPLA7* expression. To address this issue, we performed MSRE-PCR analysis using locus-specific primers for the previously reported *PNPLA7* promoter (Zhang et al., 2016) to investigate the methylation levels of the *Eag*I-CpG site in HepG2 cells cultured without methionine for 48 hours relative to those cultured with methionine. The positions of the *Eag*I-CpG site and primers used in the MSRE-PCR analysis is shown in Figure 16b. HepG2 cells cultured without methionine showed a significant reduction of the percent methylation level compared with the cells cultured with methionine (Figure 7(c)). These results suggest that the decreased SAM flux in methionine-deficient cells resulted in the reduced methylation of the *PNPLA7* promoter, thereby allowing increased *PNPLA7* expression.

The PNPLA7-dependent SAM production is linked to epigenetic regulation by modifying histone and DNA methylation

As described above, methionine is the precursor for SAM, which acts as an essential methyl donor for methylation modifications of histones and DNA and thus regulates the expression of various genes (Moghe et al., 2011; Ye et al., 2017). Since our previous study revealed that *Pnpla7* deficiency in mice decreases the hepatic production of endogenous choline from membrane PC and thereby perturbs the methyl group flux into the methionine cycle (see Introduction), it is likely that the expression of *PNPLA7* could affect cellular SAM levels *in vivo*, leading to some alterations in the profiles of histone and/or DNA methylation, although this possibility had remained to be unresolved.

To examine whether the absence of *PNPLA7* in the liver of *Pnpla7*$^{-/-}$ mice could indeed alter epigenetic modification, we first compared histone methylation between liver tissues from 6-weeks-old male *Pnpla7*$^{+/+}$ and *Pnpla7*$^{-/-}$ mice (Figure 8(a)). The results were summarized as a bar graph of representative histone modifications (Figure 8(b)) and as a heat map in global analysis with hierarchical clustering (Figure 9). The heat map generated using Z-scores amplified the changes differentially displaying histone methylation and acetylation, which highlighted an overall trend toward decreases in methylation or acetylation and reciprocal increases in unmethylation or unacetylation of corresponding histones. In particular, 35 and 26 histones out of total 92 histones were for methylation and acetylation respectively. Out of

methylation, 7 histones (20%) were downregulated over 50% and 1 histone was upregulated over 150%, and out of 26 acetylation, 8 histones (30%) were downregulated over 50% and 1 histone was upregulated over 150%. Focusing on histone methylation, there were changes in the methylation status of several histones such as increased H3:K79ME1 (mono-methylated), H3:K79ME2 (di-methylated) and H3:K36ME1 *versus* decreased H3:K79UN and H3.1:K36UN (unmethylated), in *Pnpla7*$^{-/-}$ mice relative to *Pnpla7*$^{+/+}$ mice (Figure 9). According to the bar graph (Figure 8(b)) and the heat map (Figure 9), H3:K79 and H3.1:K36 were likely to be correlated consistently with *Pnpla7* genotypes, suggesting that PNPLA7 contributes to the methylation of these histones by controlling SAM flux.

We next analyzed how DNA methylation patterns would be changed in the liver of *Pnpla7*$^{+/+}$ and *Pnpla7*$^{-/-}$ mice using RRBS for analysis of genome-wide DNA methylation (Figure 10(a)). The principle of the RRBS analysis strategy is illustrated in Figure 10(b) (see also Materials and Methods). Methylation data were generated using next-generation sequencing (NGS). Using the RRBS analysis in the promoter 2K region, total 19,703 genes were identified to be methylated in the livers of *Pnpla7*$^{+/+}$ and *Pnpla7*$^{-/-}$ mice. Scatter plot with the regression line ($y = 0.9906\ x + 0.0042$) showed the ratio of methylation levels of individual genes in the liver of *Pnpla7*$^{-/-}$ mice relative to *Pnpla7*$^{+/+}$ mice (Figure 11(a)). To select a set of genes whose methylation levels were downregulated over 15% in the liver of *Pnpla7*$^{-/-}$ mice compared to that of *Pnpla7*$^{+/+}$ mice, a new threshold was set by shifting the regression line for

15% in the X axis (y = 0.9906 x – 0.15). Total 83 genes in the lower right met this criterion (Figure 11(b)), implying that the promoter methylation of the 83 genes was decreased in *Pnpla7*$^{-/-}$ mice relative to *Pnpla7*$^{+/+}$ mice.

Considering that the decreased DNA methylation is often associated with enhanced gene expression, we next performed microarray gene profiling of the livers from *Pnpla7*$^{+/+}$ and *Pnpla7*$^{-/-}$ mice (using a pool of 4 mice for each genotype) to select particular genes whose expression levels were profoundly affected by *Pnpla7* deficiency. The results of the microarray analysis revealed significant increases (Table2(a)) and decreases (Table2(b)) in the expression of a number of genes in the livers from *Pnpla7*$^{-/-}$ mice relative to *Pnpla7*$^{+/+}$ mice. Fold changes in *Pnpla7*$^{-/-}$ mice relative to those in *Pnpla7*$^{+/+}$ mice were calculated as the absolute values of gene expression levels in *Pnpla7*$^{-/-}$ mice divided by those in *Pnpla7*$^{+/+}$ mice, which represented the differences between them. These results suggest that *Pnpla7* deficiency changes the methylation status of some if not all of these genes and histones, leading to altered gene expression profiles that could be associated with phenotypic abnormalities. It is unlikely that the altered histone and DNA methylation in *Pnpla7*$^{-/-}$ mice was due to changes in the expression of histone or DNA methyltransferases, since the expression of these enzymes was not affected by *Pnpla7* deficiency on the microarray data (data not shown).

Combining the data from the RRBS (Figure 11) and microarray (Table 2) analyses, 12 particular genes whose DNA methylation levels were negatively correlated with mRNA

expression levels were selected (Figure 11(a)). These genes included *Ankrd2* and *Myo7b*, which might be related to myofibroblasts (Cenni et al., 2011; Mohamed et al., 2013), *Igfbp5*, which neutralizes IGF-1 (Weng et al., 2019), *Ralgps1*, which is a member of *Ral* GTPase-activating proteins (A et al., 2016), *Ctcfl* and *Ccdc105*, which might be associated with hepatocarcinoma (He et al., 2017), *Klhdc1*, which might be related to hepatic redox regulation (Chin et al., 2007), and several other genes with unknown functions (Table 3). Indeed, the increased expression (Figure 12(a)) was associated with reduced DNA methylation (Figure 12(b)) of these genes in *Pnpla7*$^{-/-}$ mice relative to *Pnpla7*$^{+/+}$ mice. These results suggest that the altered methyl group flux through the PNPLA7-driven PC catabolism and methionine cycle via SAM might have some effects on hepatic fibrosis, growth, signal transduction, oncogenic transformation, and redox regulation through epigenetic regulation.

Expression of PNPLA7 and related enzymes in human hepatocellular carcinoma

Our studies using *Pnpla7*$^{-/-}$ mice and a HepG2 cell line revealed that the PNPLA7-driven PC-catabolic pathway, which is coupled with the methionine cycle, is important for endogenous SAM supplementation and thereby epigenetic regulation of gene expression (Wang et al., 2017b). Reportedly, SAM supplementation inhibits the growth, transformation, and invasion of liver cancer (Frau et al., 2012; Wang et al., 2017b). We therefore aimed to examine whether

the PNPLA7-dependent metabolic pathway, which is coupled with endogenous SAM production, would have some associations with human liver cancer.

We obtained freshly frozen liver samples of patients with hepatocellular carcinoma from the University of Tokyo Hospital (in collaboration with Drs. Yatomi and Kurano at the Department of Laboratory Medicine) and examined the expression of *PNPLA7* as well as its paralogs *PNPLA6, PNPLA8* and *PNPLA9* in the tumor and adjacent non-tumor (control) tissue by real-time PCR. We found that the expression levels of *PNPLA7* and *PNPLA8,* two enzymes participating in the PC-catabolic pathway in the liver, but not their respective homologs *PNPLA6* and *PNPLA9*, were significantly lower in tumor tissues than in non-tumor tissues (Figure 13(a)). Heat map representation revealed that *PNPLA7* was markedly downregulated in tumor tissues relative to non-tumor tissues of most patients, with more than 90% reduction in 12 out of 54 specimens (Figure 13(b)). *PNPLA8* also showed a similar trend (although milder than *PNPLA7*), being decreased in the tumor of many patients (Figure 13(c)). The reduced expression of *PNPLA7* (Figure 14(a)) and *PNPLA8* (Figure 14(b)) in human hepatocellular carcinoma did not show appreciable correlations among the grades of hepatic fibrosis nor the etiology including the carcinoma caused by hepatitis B (HBV) infection (type B), that by hepatitis C (HCV) infection (type C), and that unlikely related to HBV/HCV infection (type non-B/non-C, likely associated with alcoholic or non-alcoholic fatty liver diseases (nonalcoholic fatty liver disease (NAFLD) or NASH)). These results imply that oncogenic

transformation may lead to downregulation of *PNPLA7* and *PNPLA8* regardless of the cause of liver cancer, although final conclusion needs further study using increased number of clinical samples for multivariate analysis. Additionally, the expression levels of *BHMT, MAT1A* and *PEMT*, which are components in the methionine cycle, were also significantly lower in the tumor samples than in the non-tumor samples (Figure 15(a)). Similar tendency was also observed with the expression of *GPCPD1* and *AHCY*, even though statistically insignificant (Figure 15(a)). Collectively, multiple enzymes in the PC catabolism and methionine cycle were concomitantly downregulated in human hepatocellular carcinoma (Figure 15(b)), suggesting a decreased metabolic flux through this pathway.

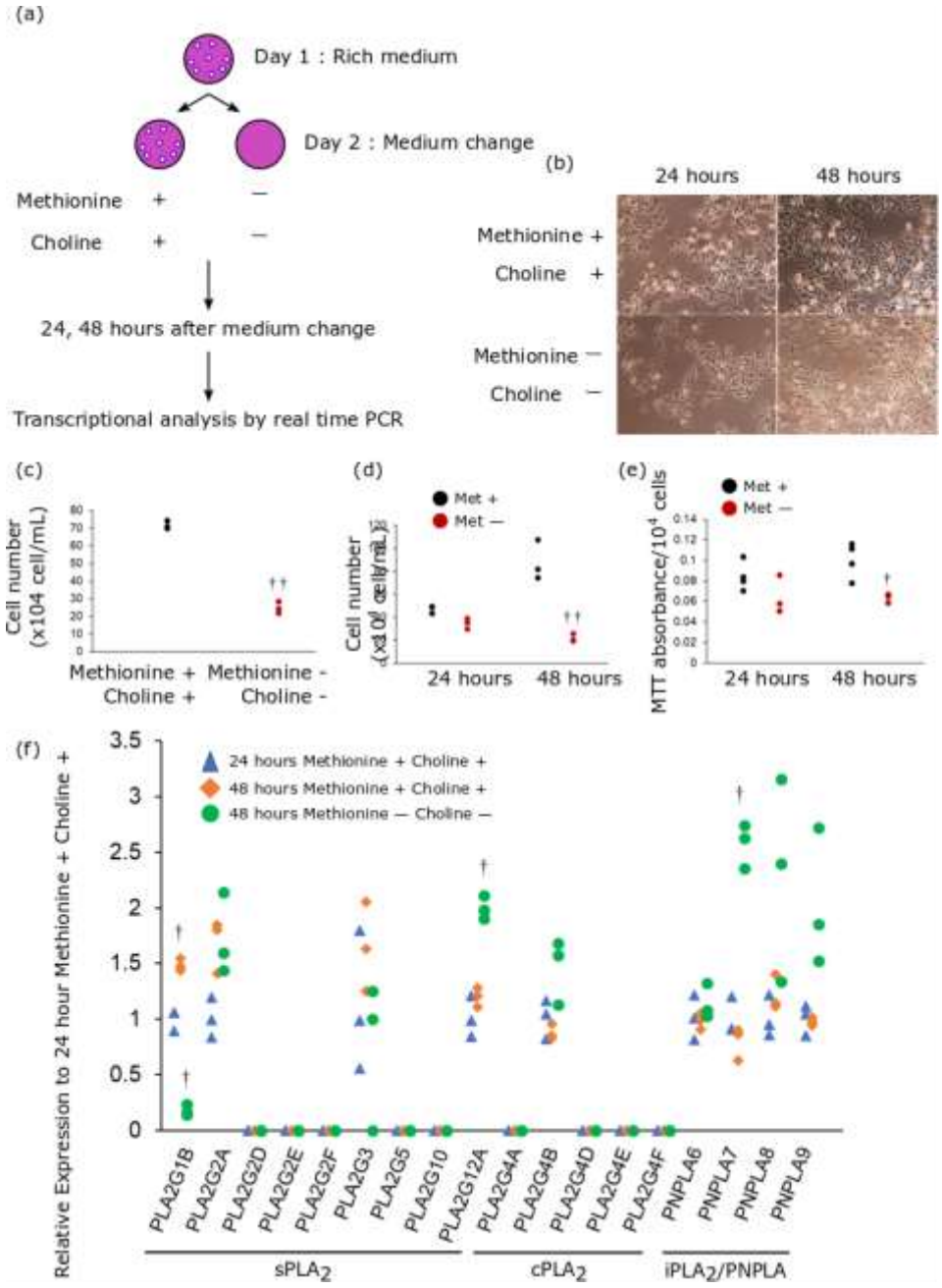

Figure 3. Effects of choline and/or methionine deficiency on proliferation and PLA_2 gene expressions in HepG2 cells. (a) Experimental procedure. The cells were cultured in D-MEM/Ham's F-12 medium with or without methionine and choline for 24 or 48 hours. (b) Images of HepG2 cells after culturing for 24 and 48 hours with or without choline and methionine. (c) Cell counts of HepG2 cells cultured with or without methionine and choline for 48 hours as assessed by trypan blue dye exclusion (n = 3). (d, e) Cell counts of HepG2 cells cultured with or without methionine for 24 hours and 48 hours as assessed by trypan blue dye exclusion (d) or MTT assay (e) (n = 3 for cell count, n = 4 for MTT assay). (f) Relative expressions of various secreted PLA_2, cytosolic PLA_2, and PNPLA/ $iPLA_2$ enzymes. (n = 3; †, $P < 0.05$; ††, $P < 0.01$ *versus* HepG2 cells cultured with Methionine + Choline + for 24 hours by two-tailed Student's t-test). Data, mean ± SEM. N.D., Not Detected.

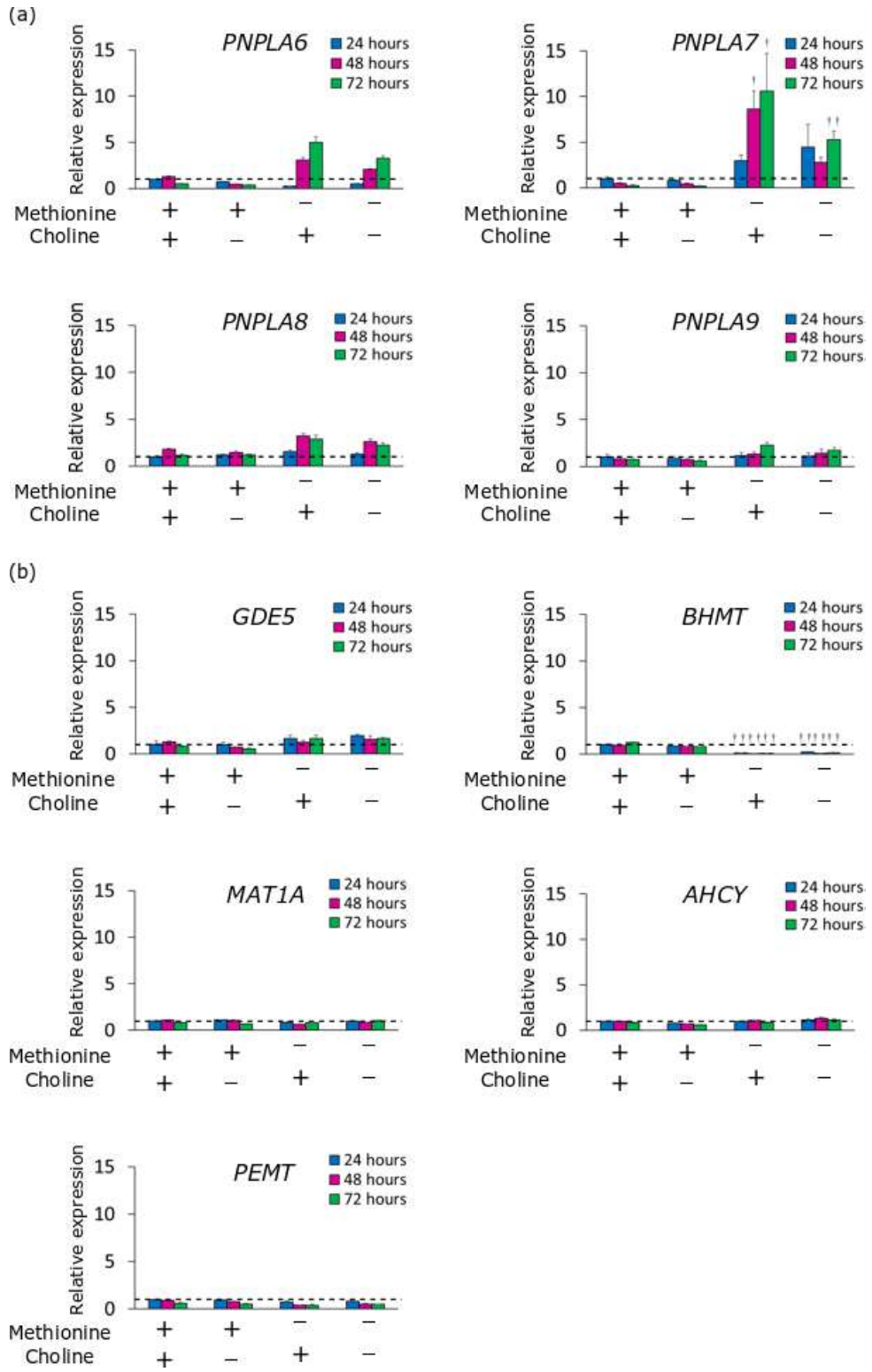

Figure 4. Relative expression of (a) PNPLA/iPLA$_2$ enzymes and (b) enzymes involved in choline and methionine cycle in HepG2 cells cultured for 24, 48, and 72 hours with choline-free, methionine-free, or choline/methionine-free medium. Dashed lines indicate the expression level of each gene under normal culture condition. (n = 6; †, $P < 0.05$; ††, $P < 0.01$ *versus* HepG2 cells cultured with Methionine + Choline + for 24 hours by two-tailed Student's t-test). Data, mean ± SEM.

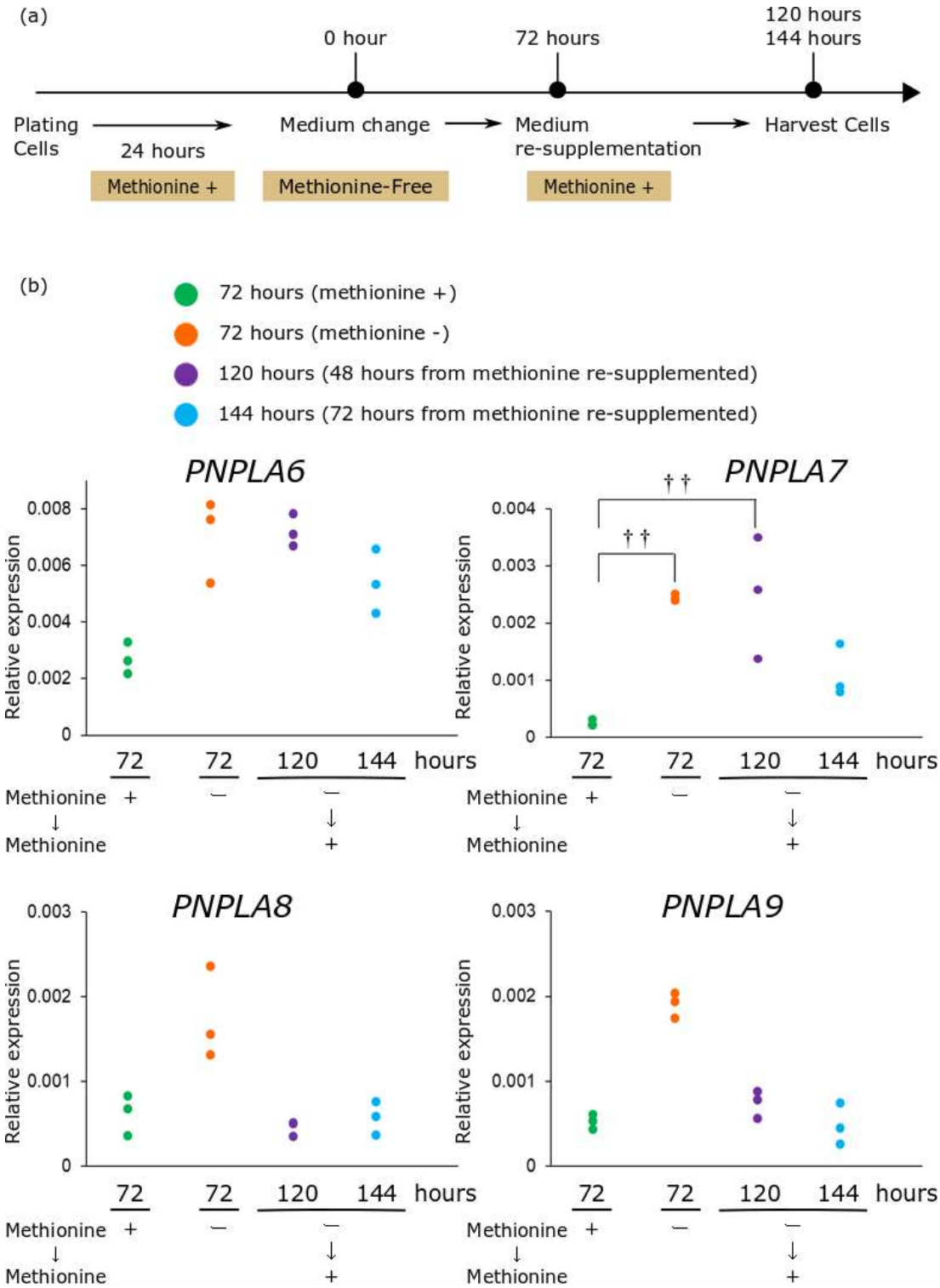

Figure 5. The effects of methionine re-supplementation on the expression of *PNPLA7* and related enzymes. (a) Experimental scheme. HepG2 cells that had been cultured for 72 hours in methionine-free medium were then cultured for the indicated times in medium supplemented with methionine. (b) Real-time PCR of PNPLA/iPLA$_2$ enzymes upon methionine restriction and re-supplementation. The y-axis shows the relative expression to gene expression cultured with methionine for 72 hours. Dashed lines indicate the expression level of each gene under normal condition. Data, mean ± SEM; ††, $P < 0.01$, ANOVA with Turkey post hoc test

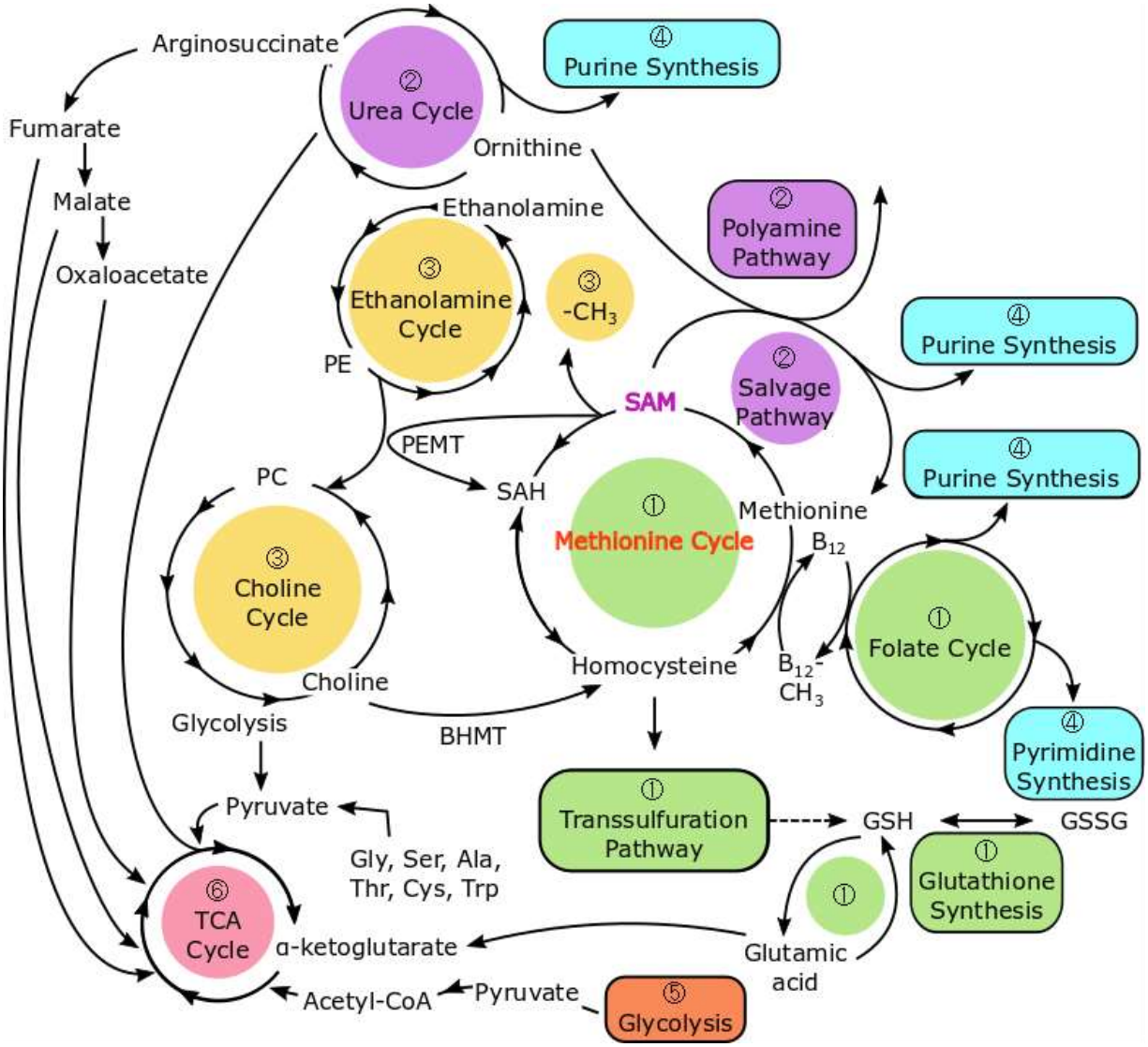

Figure 6 (a)**.** An overview of the metabolic pathways related to the methionine cycle. Details and results of the methionine cycle, transsulfuration pathway, glutathione synthesis, and folate cycle are indicated in Figure 6 (b), the salvage pathway, polyamine pathway, and urea cycle are indicated in Figure 6 (c), the choline and ethanolamine cycle are indicated in Figures 6 (d) and 6 (e), the purine and pyrimidine synthetic pathways are indicated in Figure 6 (f), and glycolysis is indicated in Figure 6 (g), and the TCA cycle is indicated in Figure 6 (h).

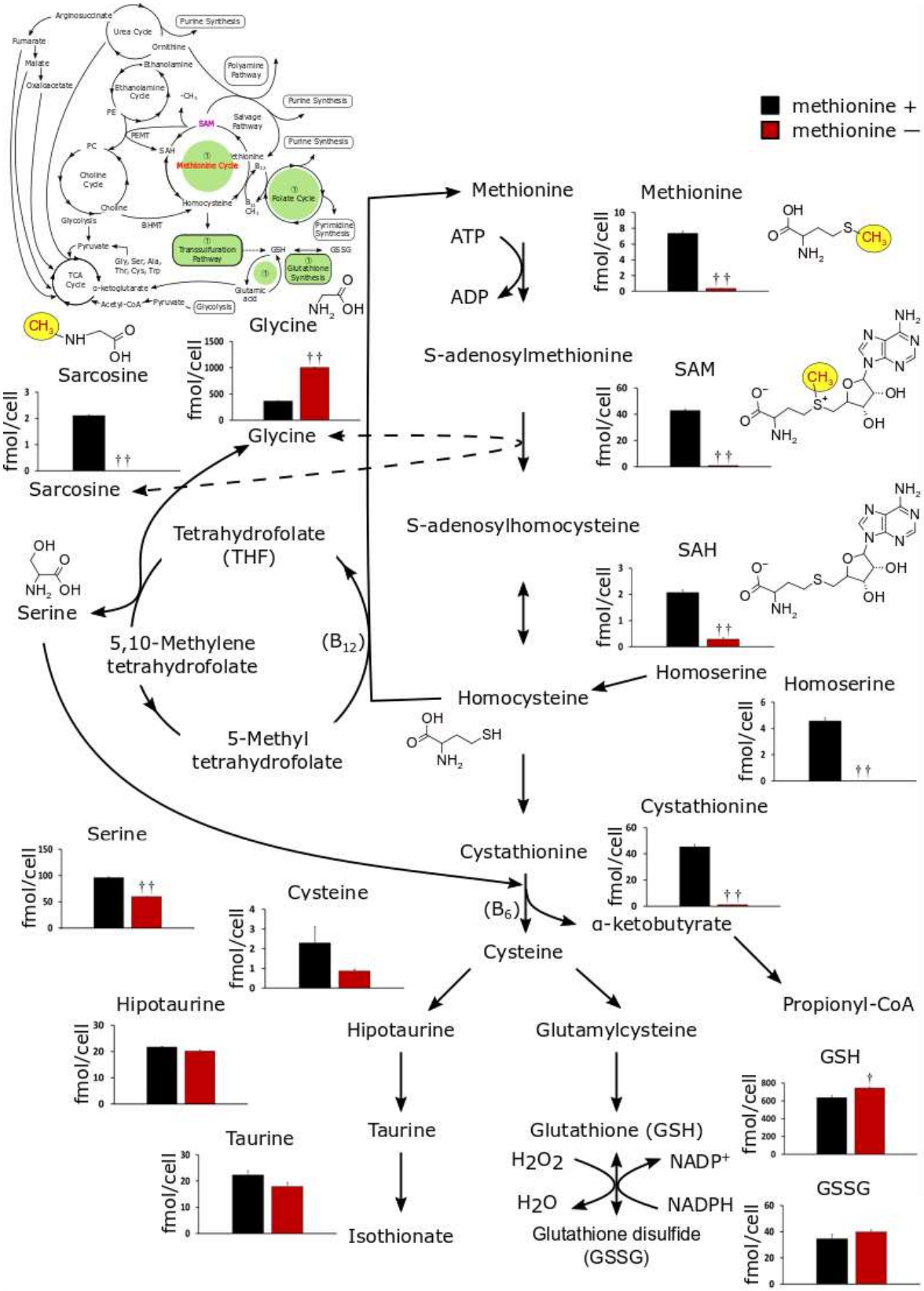

Figure 6 (b)**.** Schematic representation of the methionine cycle, transsulfuration pathway, and folate cycle. Bar graphs represent the concentrations of individual metabolites in HepG2 cells cultured with (black) or without (pink) methionine for 48 hours (n = 4). Data, mean ± SEM; †, $P < 0.05$; ††, $P < 0.01$ *versus* cells cultured with methionine-sufficient medium.

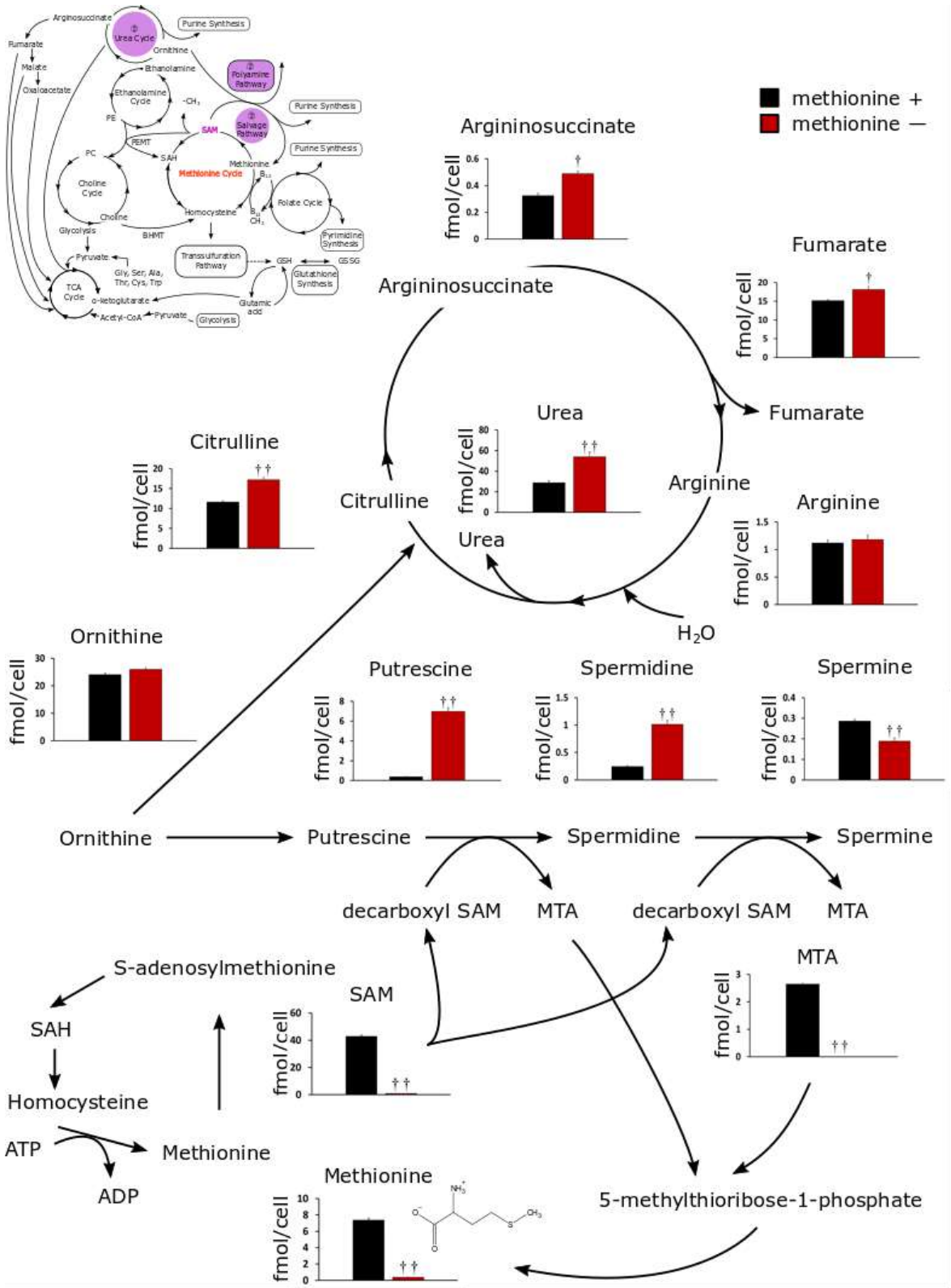

Figure 6 (c)**.** Schematic representation of the methionine salvage pathway, polyamine pathway and urea cycle in connection with the methionine cycle. Bar graphs represent the levels of individual metabolites in HepG2 cells cultured with (black) or without (red) methionine for 48 hours (n = 4). Data; mean ± SEM; †, $P < 0.05$; ††, $P < 0.01$ *versus* cells cultured with methionine-sufficient medium.

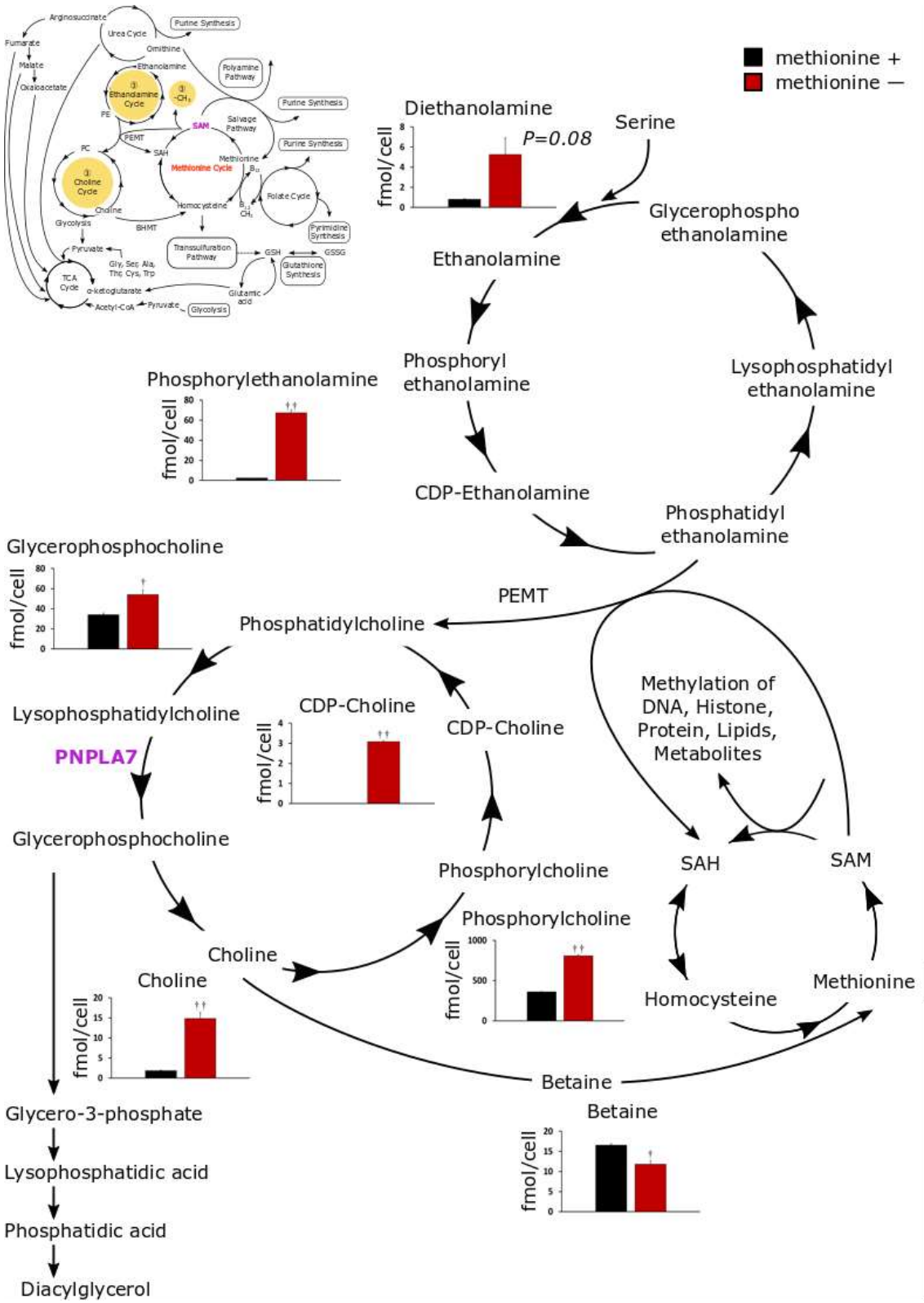

Figure 6 (d)**.** Schematic representation of choline and ethanolamine metabolisms in the Kennedy pathway and their association with the methionine cycle. Bar graphs represent the levels of individual metabolites in HepG2 cells cultured with (black) or without (red) methionine for 48 hours (n = 4). Data, mean ± SEM; †, $P < 0.05$; ††, $P < 0.01$ *versus* cells cultured with methionine-sufficient medium.

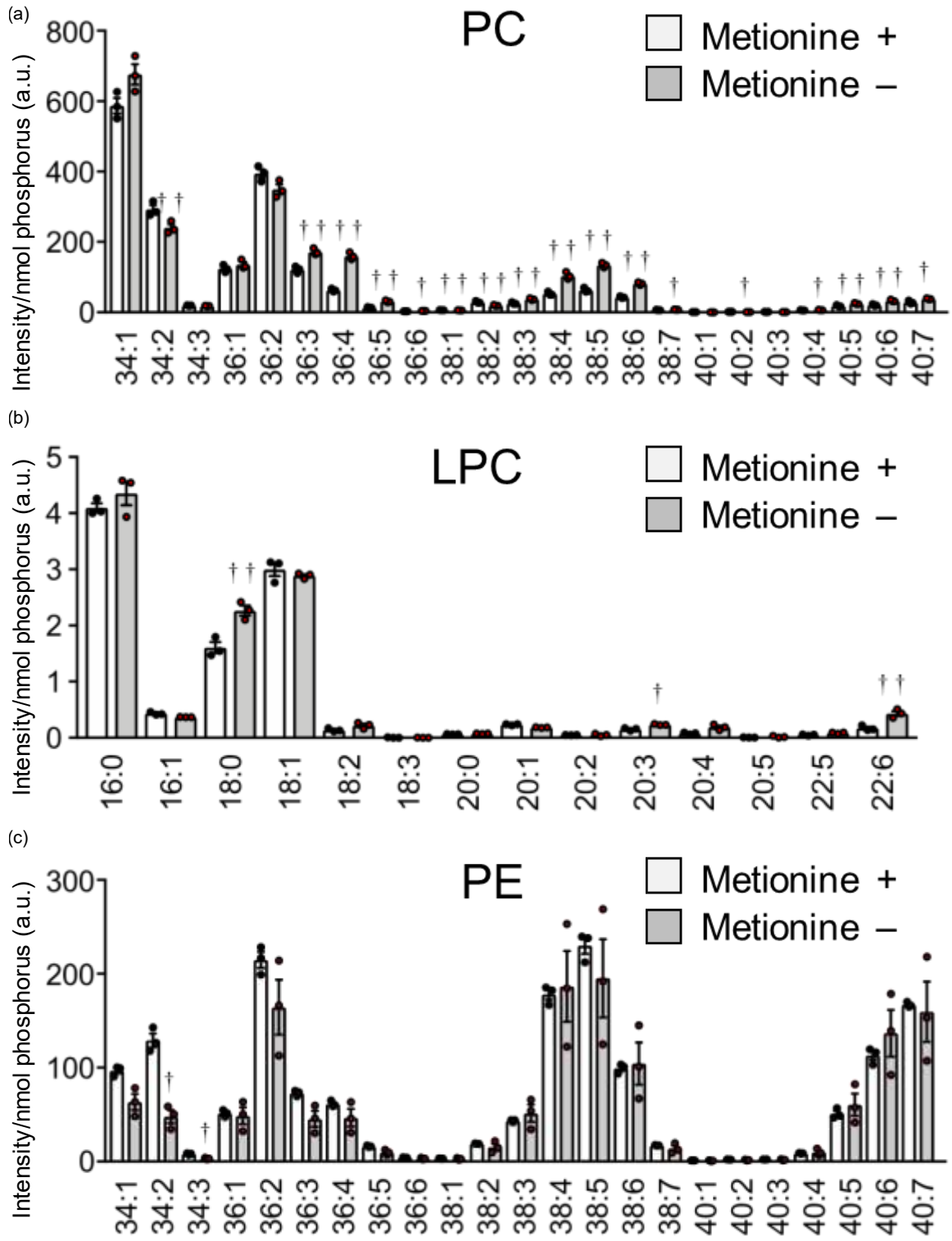

Figure 6 (e)**.** Lipidomics of (a) PC, (b) LPC, and (c) PE in HepG2 cells cultured with or without methionine for 48 hours. Bar graphs represent the levels of individual lipid molecular species in HepG2 cells cultured with (white) or without (gray) methionine for 48 hours (n = 3). Numbers in the x-axis represent different molecular species (carbon number: double bond number of fatty acyl chains) of PC, LPC and PE. Data, mean ± SEM; †, $P < 0.05$; ††, $P < 0.01$ *versus* cells cultured with methionine-sufficient medium.

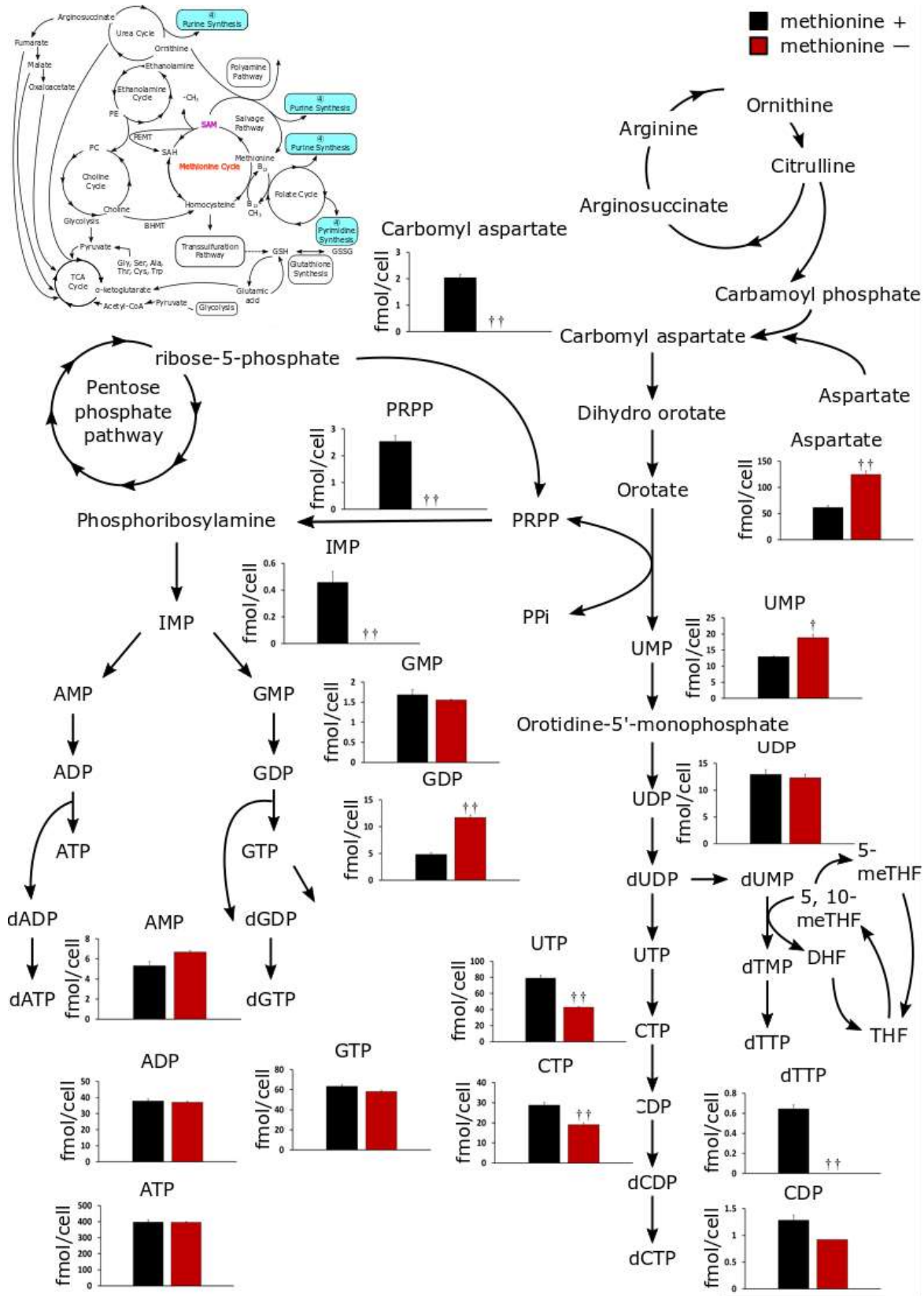

Figure 6 (f)**.** The *de novo* synthesis of purine and pyrimidine. Bar graphs represent the levels of individual metabolites in HepG2 cells cultured with (black) or without (red) methionine for 48 hours (n = 4). Data, mean ± SEM; †, $P < 0.05$; ††, $P < 0.01$ *versus* cells cultured with methionine-sufficient medium.

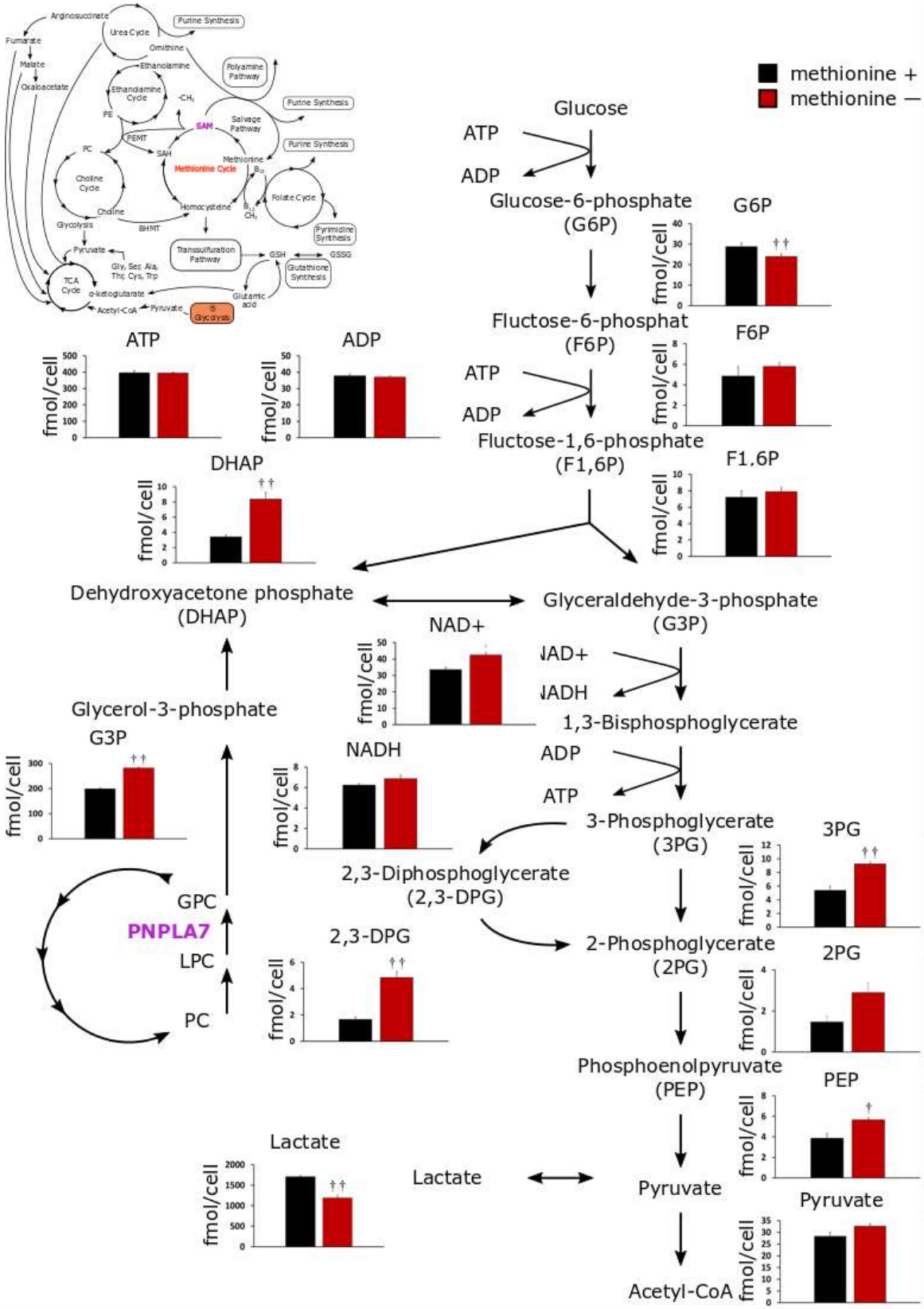

Figure 6 (g)**.** Schematic representation of glycolysis. Bar graphs represent the levels of individual metabolites in HepG2 cells cultured with (black) or without (red) methionine for 48 hours (n = 4). Data, mean ± SEM; †, $P < 0.05$; ††, $P < 0.01$ *versus* cells cultured with methionine-sufficient medium.

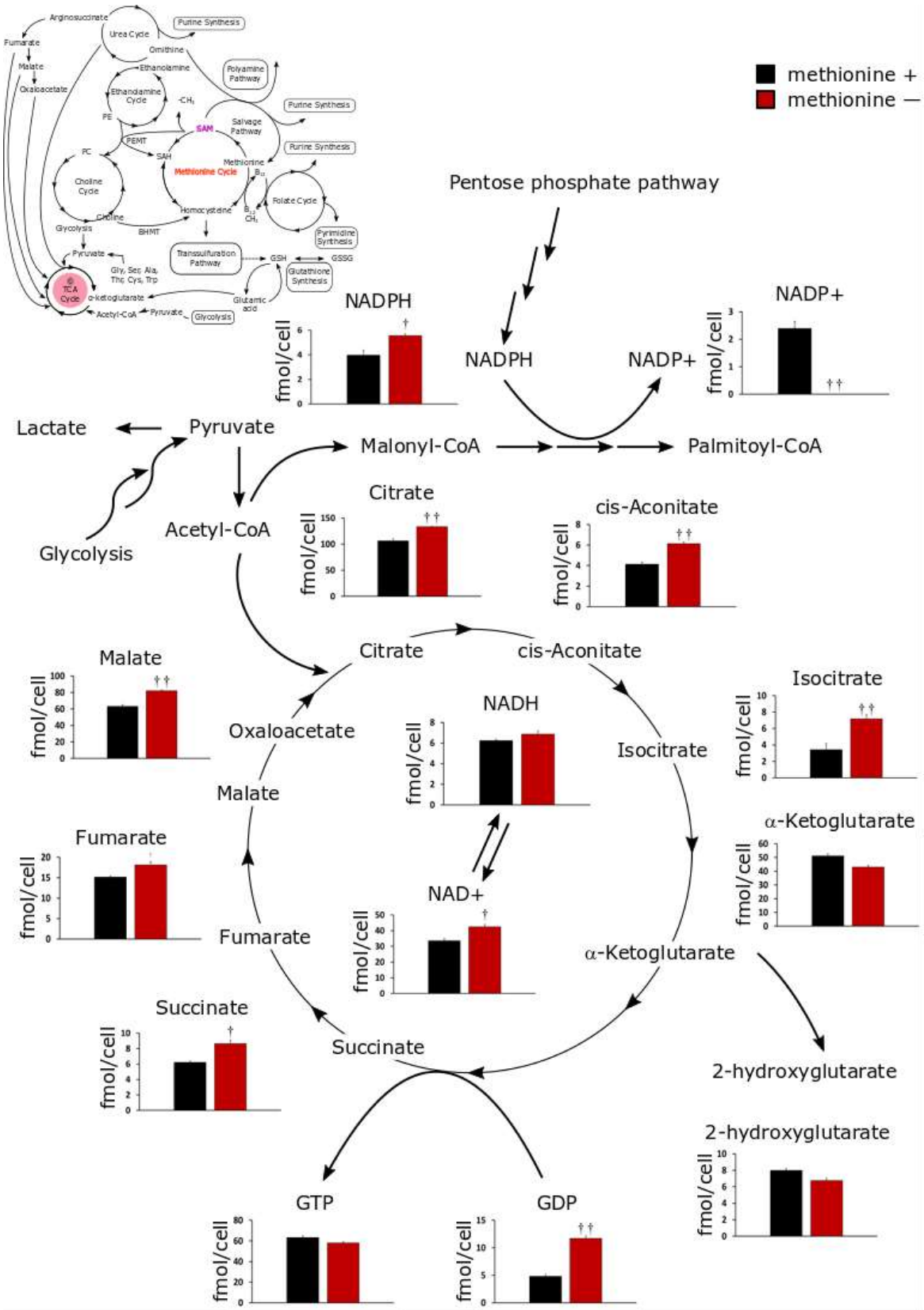

Figure 6 (h)**.** Schematic representation of the TCA cycle. Bar graphs represent the levels of individual metabolites in HepG2 cells cultured with (black) or without (red) methionine for 48 hours (n = 4). Data, mean ± SEM; †, $P < 0.05$; ††, $P < 0.01$ *versus* cells cultured with methionine-sufficient medium.

(a)

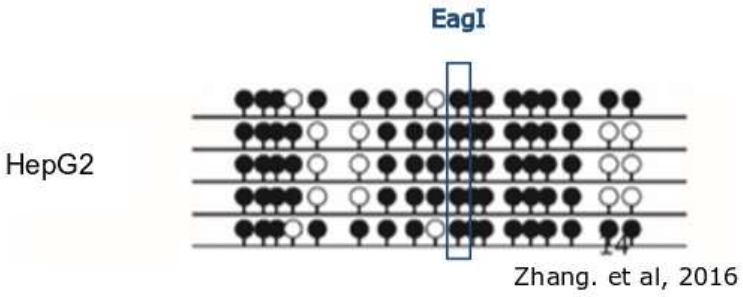

(b)

GTGCGGACCGAATGAGCAAGTGGACGAGCAAGCGGGGCCCGCGCA
GCTTCAGGGGCCGCAAGGGCCGGGGCGCCAAGGGCATCGGCTTCCT
CACCTCGGGCTGGAGGTTCGTGCAGATCAAGGAGATGGTCCCGGAG
TTCGTCGTCCCGGATCTGACCGGCTTCAAGCTCAAGCCCTACGTGAG

EagI

CTACCTCGCCCCTGAGAGCGAGGAGACGCCCCTGACGGCCGCGCAG
CTCTTCAGCGAAGCCGTGGCGCCTGCCATCGAAAAGGACTTCAAGG
ACGGTACCTTCGACCCTGACAACCTGGAAAAGTACGGCTTCGAGCC
CCACACAGGAGGGAAAGCTCTTCCAGCTCTACCCCAGGAACTTCCT
GCGCTAGC

Primer

MSRE-PCR-PNPLA7-F1 : GGTTCGTGCAGATCAAGGAG
MSRE-PCR-PNPLA7-R2 : GTTGTCAGGGTCGAAGGTACC

(c)

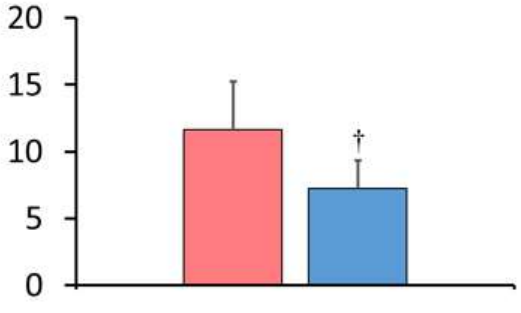

Figure 7. Scheme of the MSRE-PCR analysis of the *PNPLA7* promoter. (a) Methylation status of the *PNPLA7* promoter in HepG2 cells (Zhang et al., 2016). (b) Promoter sequence of the *PNPLA7* gene for the MSRE-PCR amplification. Sequences highlighted with yellow and blue are the primer regions used for PCR amplification. The short vertical line shows the cleavage site of *Eag*I. (c) Bar graph showing frequency of the methylated CpG site in the *PNPLA7* promoter in HepG2 cells cultured with or without methionine (n = 4). Data, mean ± SEM; †, $P < 0.05$; ††, $P < 0.01$ *versus* cells cultured with methionine-sufficient medium.

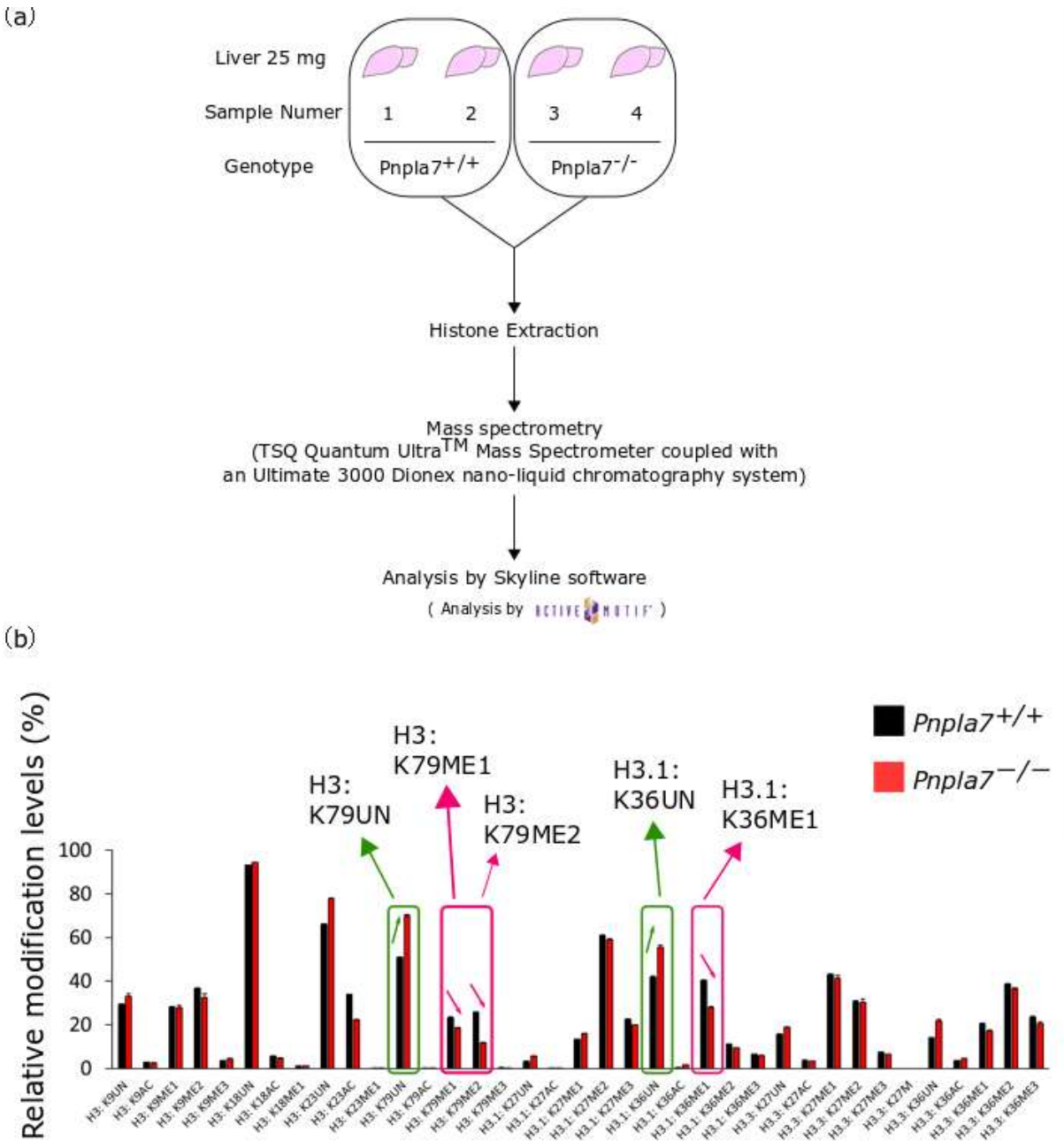

Figure 8. Analysis of histone modifications in the livers of *Pnpla7*$^{+/+}$ and *Pnpla7*$^{-/-}$ mice. (a) A schematic procedure. Liver samples (25 mg) from *Pnpla7*$^{+/+}$ (WT) and *Pnpla7*$^{-/-}$ (KO) mice were analyzed for histone modifications (methylation and acetylation) by a Mod Spec^{R} method (Active Motif) in order to get a broader overview of histone modification profiles. Histone extraction, protease digestion, and mass spectrometry using a triple quadrupole (QqQ) Mass Spectrometer (Thermo Scientific TSQ Quantiva) directly coupled with an UltiMate 3000 Dionex nano-liquid chromatography system were performed by Active Motif. All the processes were done in duplicate and the data were analyzed by Skyline with Savitzky-Golay smoothing. (b) Quantification of representative histone modifications in *Pnpla7*$^{+/+}$ (black) and *Pnpla7*$^{-/-}$ (red) mice (n = 2; Data, mean ± SD). Increased and decreased histone modifications in *Pnpla7*$^{-/-}$ mice relative to *Pnpla7*$^{+/+}$ mice are highlighted in green and red boxes, respectively.

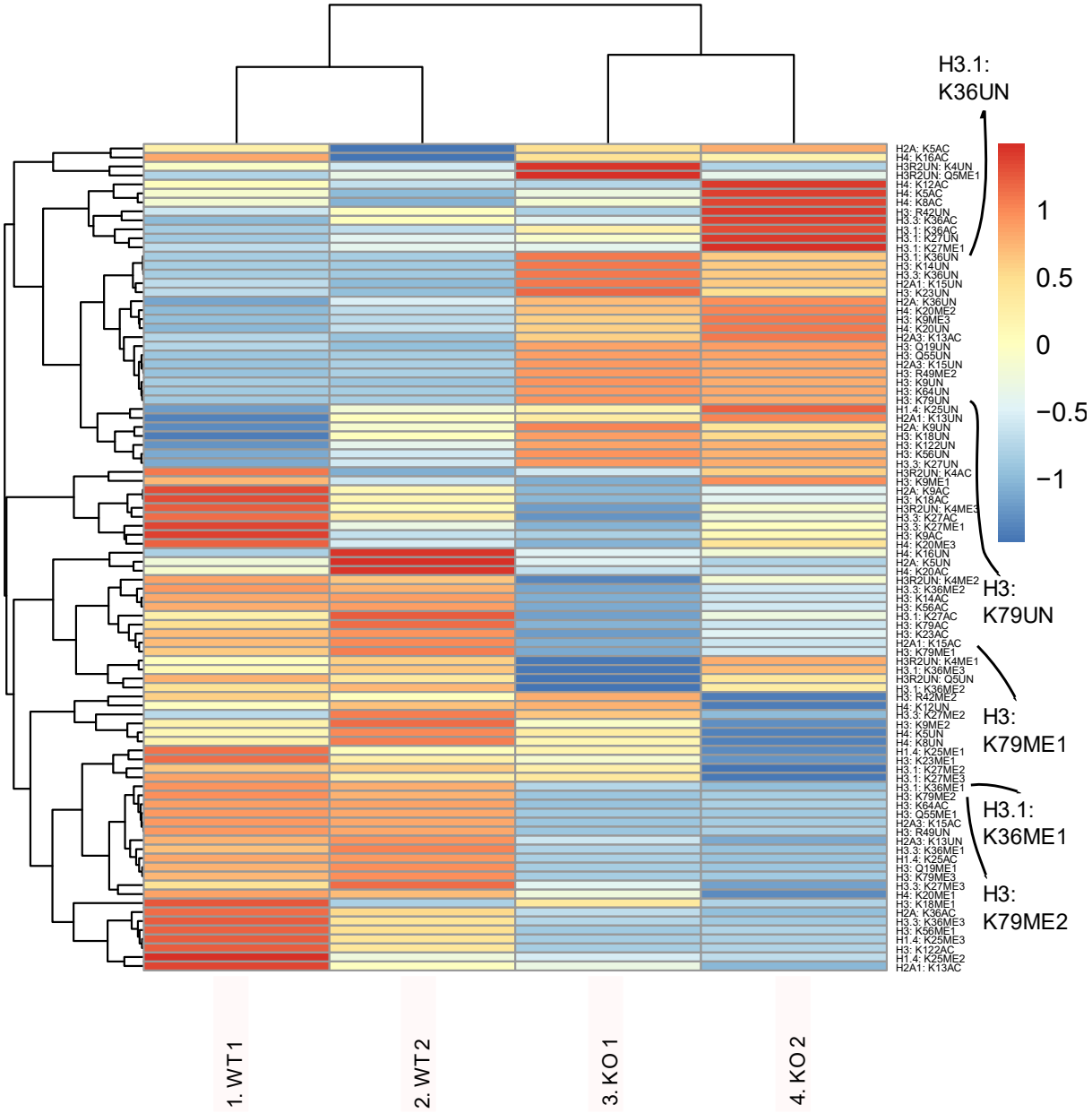

Figure 9. Heat map representation of histone modifications with hierarchical clustering. Higher and lower levels of individual histone modifications are shown in red and blue, respectively. Modifications of H3.1:K36 and H3:K79 (see Figure 8) are highlighted.

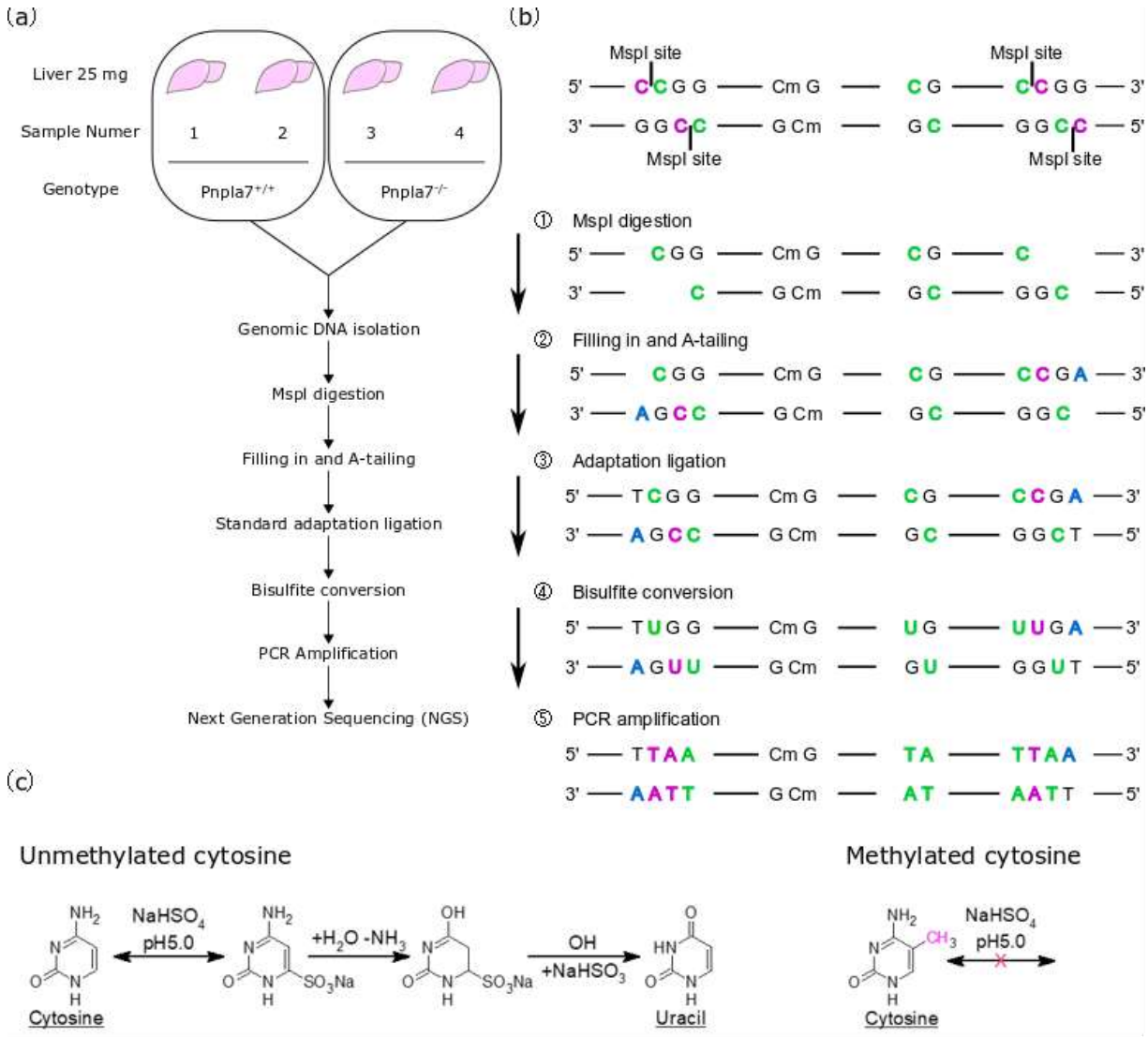

Figure 10. Analysis of DNA methylation in the livers of *Pnpla7*$^{+/+}$ and *Pnpla7*$^{-/-}$ mice. (a) A schematic procedure. Genomic DNA extracted from liver samples (25 mg) from *Pnpla7*$^{+/+}$ and *Pnpla7*$^{-/-}$ mice was analyzed by a RRBS method (Active Motif) in order to get a broader overview of DNA methylation profiles. DNA samples were taken for *Msp*I digestion, filling in and A-tailing, sequencing adapter ligation, bisulfite conversion, PCR amplification, next generation sequencing, and bioinformatic analysis. (b) The principle of RRBS methodology. (c) Chemical reaction underlying the bisulfite-catalyzed conversion of cytosine to uracil.

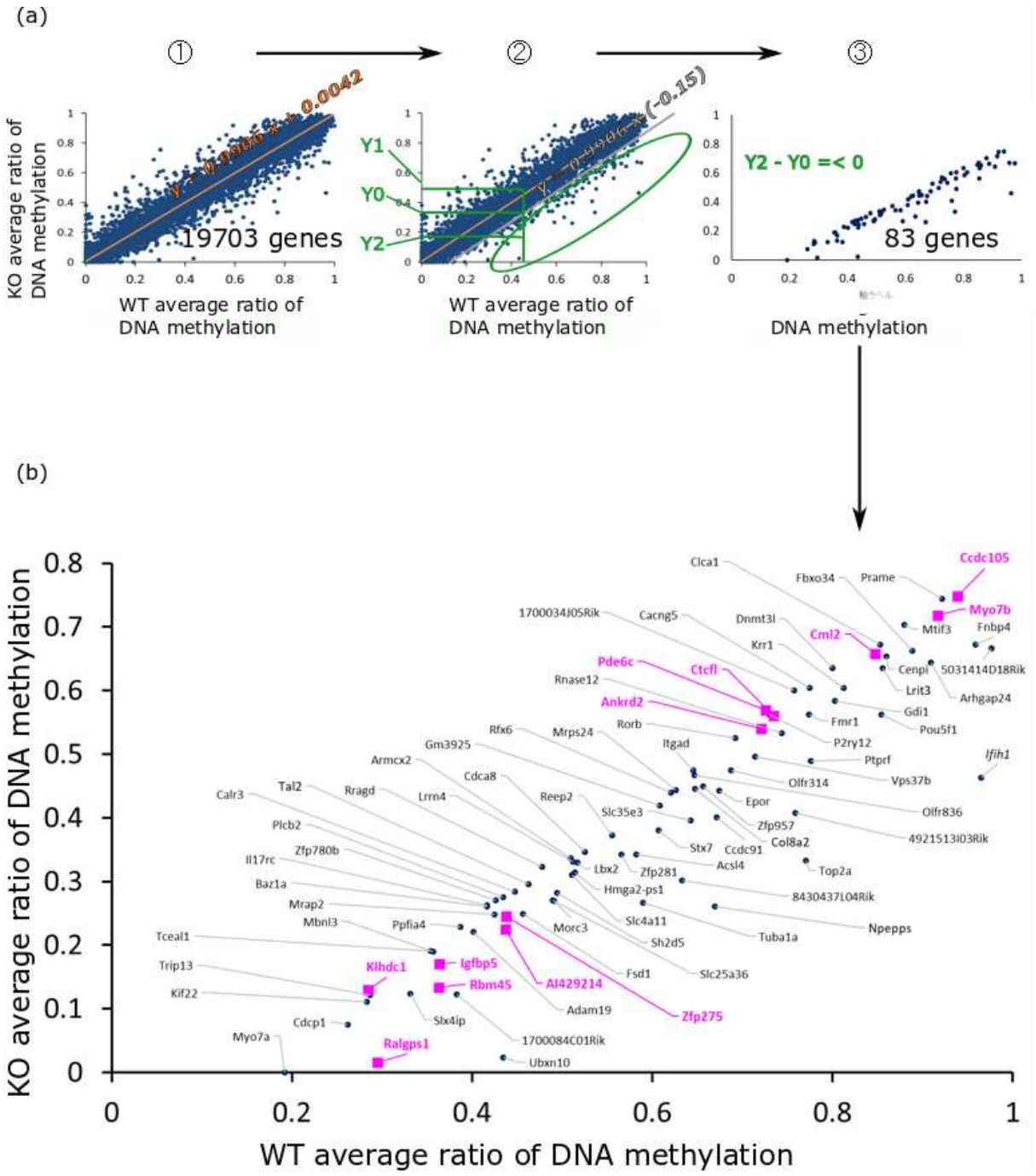

Figure 11. Scattered plot of DNA methylation in the livers from *Pnpla7*$^{+/+}$ (WT) and *Pnpla7*$^{-/-}$ (KO) mice. (a) ①The levels of DNA methylation in the CpG sites (within 2K from the translation initiation sites) of 19,703 total genes are plotted. ②The regression line (y = 0.9906 x + 0.0042) is parallelly shifted for 15 % in the X axis (y = 0.9906 x - 0.15). ③83 genes in the lower right under the new threshold were selected as those with reduced DNA methylation in KO mice relative to WT mice. (b) Magnified visualization of the scatter plot for the 83 genes with individual gene names. Among them, the genes elevated in KO mice relative to WT mice in the microarray analysis (Figure 12) are highlighted by pink squares.

Table 2. (a) The top 50 upregulated genes in microarray analysis of the livers from *Pnpla7*$^{-/-}$ mice relative to *Pnpla7*$^{+/+}$ mice.

No.	Gene Name	Accession #	Found Value (*Pnpla7*$^{-/-}$)	Found Value (*Pnpla7*$^{+/+}$)	Fold Change
1	*Sult1e1*	NM_023135	17186.66	25.79	724.55
2	*AI428406*	BX520338	749.18	3.23	252.01
3	*Sln*	NM_025540	1308.23	6.25	227.79
4	*Il13*	NM_008355	713.44	3.48	223.01
5	*Myot*	NM_001033621	959.62	4.82	216.66
6	*Mlip*	AK009836	528.93	3.44	167.21
7	*Actn2*	NM_033268	524.68	4.04	141.23
8	*Gm20758*	NR_046029	411.01	3.24	137.79
9	*Gabrg3*	NM_008074	359.07	3.41	114.45
10	*Sgpp2*	NM_001004173	341.39	3.48	106.78
11	*Myl1*	NM_021285	5897.07	61.38	104.48
12	*Myh2*	NM_001039545	6059.74	63.16	104.33
13	*Ttn*	NM_011652	664.65	7.08	102.08
14	*Myl1*	NM_001113387	280.79	3.02	100.99
15	*Gm13280*	NM_206867	313.99	3.39	100.66
16	*Agbl4*	AK016502	317.03	3.44	100.34
17	*Ckm*	NM_007710	421.01	4.69	97.61
18	*Ckmt2*	NM_198415	3469.98	39.83	94.75
19	*6530403M18Rik*	XR_168590	275.80	3.26	92.03
20	*LOC100862557*	XM_003689292	2406.17	29.49	88.72
21	*Nmrk2*	NM_027120	1586.49	19.80	87.12
22	*Tmem8b*	NM_001085508	642.99	8.06	86.77
23	*Akap4*	NM_001042542	269.16	3.39	86.29
24	*Myh8*	NM_177369	7518.75	94.81	86.24
25	*E030018B13Rik*	NM_001256311	246.78	3.14	85.39
26	*Tnnt3*	NM_001163664	2822.56	36.32	84.50
27	*Myh4*	NM_010855	243.38	3.20	82.59
28	*Gm2016*	NM_001122662	259.19	3.43	82.18
29	*Mageb16*	NM_028025	258.99	3.44	81.94
30	*Cntn2*	NM_177129	247.56	3.55	75.82
31	*Fam170a*	NM_001004061	284.22	4.13	74.80
32	*Arhgap15*	NM_001025377	618.61	9.06	74.24
33	*AU022434*	BG068260	215.34	3.26	71.82
34	*Scgb2b24*	NM_177446	236.32	3.70	69.41
35	*Gapt*	NM_177713	204.42	3.29	67.60
36	*Plac8l1*	NM_027072	196.83	3.17	67.49
37	*Defa3*	NM_007850	186.78	3.13	64.91
38	*Myh1*	NM_030679	2250.62	38.02	64.37
39	*Olfr1066*	NM_001011735	201.73	3.42	64.06
40	*Cnih3*	NM_028408	200.03	3.42	63.59
41	*Mb*	NM_013593	3243.66	55.55	63.50
42	*Myl2*	NM_010861	1460.60	25.44	62.43
43	*1700084K02Rik*	AK006995	183.70	3.24	61.64
44	*A630038E17Rik*	AK039976	227.20	4.05	61.05
45	*Igkv3-4*	BC108385	198.92	3.55	60.92
46	*Eif2s3x*	AK171317	277.25	5.01	60.17
47	*Cox6a2*	NM_009943	4317.37	79.54	59.03
48	*Tmem91*	NM_177102	237.81	4.38	58.97
49	*Tnnc2*	NM_009394	12217.42	227.88	58.30
50	*Sntg1*	NM_027671	351.36	6.86	55.70

Table 2. (b) The top 50 downregulated genes in microarray analysis of the livers from *Pnpla7*$^{-/-}$ mice relative to *Pnpla7*$^{+/+}$ mice.

No.	Gene Name	Accession #	Found Value (*Pnpla7*$^{-/-}$)	Found Value (*Pnpla7*$^{+/+}$)	Fold Change
1	*Ppp5c*	NM_011155	3.5753233	2140.1873	-550.4703
2	*Pcdh15*	NM_001142746	3.5364797	1654.8086	-430.30252
3	*Tppp2*	NM_001128634	3.303585	739.06	-205.72716
4	*Adamts16*	NM_172053	3.9509537	562.5887	-130.94427
5	*Henmt1*	NM_025723	3.369843	460.92758	-125.782524
6	*A330032B11Rik*	NR_045329	3.2952247	437.701	-122.14898
7	*1700042B14Rik*	NM_001081671	3.3565273	405.689	-111.1477
8	*Gm266*	NM_001033248	3.9365058	424.86612	-99.25186
9	*Kcnq2*	NM_010611	3.5640137	382.2948	-98.64077
10	*A1bg*	NM_001081067	3.693183	357.4151	-88.99578
11	*Fam24a*	NM_183272	3.4727778	325.28705	-86.13649
12	*Dbh*	NM_138942	3.6989238	345.04944	-85.783394
13	*Serpinb13*	NM_172852	3.483787	317.31134	-83.75899
14	*Kcnk12*	NM_199251	5.784019	514.9547	-81.87226
15	*Xaf1*	NM_001037713	8.111228	690.2458	-78.25544
16	*Proser1*	NM_173382	9.543171	796.4288	-76.74526
17	*Lgals7*	NM_008496	3.4289343	281.8317	-75.58367
18	*1700016D02Rik*	AK006017	3.5609658	291.7161	-75.33382
19	*D16Ertd519e*	NR_040474	3.583245	286.0911	-73.42184
20	*Pkd2l2*	NM_016927	3.548257	277.7855	-71.99328
21	*Vmn2r17*	NM_001104628	3.2583332	254.47746	-71.82097
22	*Cbx8*	NM_013926	4.1149507	288.39468	-64.449554
23	*Kcnc1*	NM_008421	5.8190165	404.5153	-63.926765
24	*Gm10631*	AK135158	431.08176	29494.121	-62.91775
25	*Frmd7*	NM_001190332	4.4502387	300.5608	-62.107826
26	*Ctse*	NM_007799	16.249372	1090.1991	-61.69736
27	*Slc36a3*	NM_172258	3.2682498	215.24985	-60.565468
28	*Gm4311*	AK035331	3.7837021	241.95482	-58.80505
29	*Slc4a10*	NM_001242380	3.706111	226.98515	-56.321793
30	*Pbsn*	NM_017471	3.9774892	240.21758	-55.53839
31	*Stk32b*	NM_022416	4.456497	255.19002	-52.658363
32	*Dtl*	AB095736	4.3932147	248.94627	-52.109947
33	*Eif1*	NM_011508	278.24936	15605.713	-51.575905
34	*4732456N10Rik*	NM_177717	3.6545799	203.88837	-51.30415
35	*Lce1i*	NM_029667	3.3745158	182.36842	-49.697613
36	*E030019B13Rik*	NR_045082	3.5741422	193.04507	-49.668877
37	*Ctps2*	AK161564	4.1596956	223.85265	-49.487804
38	*4933422H20Rik*	NM_001033775	3.5975807	190.79349	-48.76974
39	*Ano5*	NM_177694	3.546602	187.7356	-48.677883
40	*Zfp423*	NM_033327	4.356329	227.63954	-48.053444
41	*C87977*	NM_001177542	5.8263717	301.76822	-47.629135
42	*Tubgcp4*	AK051517	6.949092	353.6015	-46.793274
43	*Ccdc39*	NM_026222	3.5929317	174.6082	-44.69028
44	*Gm9946*	XR_105018	3.375063	157.16986	-42.82376
45	*1700123I01Rik*	AK028710	5.0540977	233.76607	-42.533894
46	*F2rl1*	NM_007974	11.207319	469.2439	-38.50298
47	*Pitpnm3*	NM_001024927	4.089871	169.24281	-38.05381
48	*Trex2*	NM_011907	10.334861	423.898	-37.718483
49	*Iqca*	NM_029122	4.840788	198.23262	-37.657932
50	*Olfr784*	NM_146729	3.389642	138.27489	-37.51343

Table 3. The top 12 genes upregulated in the DNA methylation (Figure 11) and downregulated in microarray (Table 2) analyses in the liver of *Pnpla7*$^{-/-}$ (KO) mice relative to *Pnpla7*$^{+/+}$ (WT) mice. The first column indicates the names of genes. The second column provides a description of each gene. The third column indicates the methylation differences as a result of (KO-WT). The fourth column indicates the gene expression levels as a result of [KO/WT]. The fifth column provides the properties and possible functions of the gene products.

Genes	Description	Methylated Difference (KO-WT)	Gene Expression [KO/WT]	Properties Possible functions
Ankrd2	Ankyrin Repeat Domain 2	-0.180652	34.52029	Related to myofiblasts?
Myo7b	myosin VIIB	-0.198810	25.979774	Related to myofiblasts
Pde6c	phosphodiesterase 6C, cGMP specific, cone, alpha prime	-0.156972	15.009336	Causal gene for achromatopsia Function in the liver is unknown
Igfbp5	insulin-like growth factor binding protein 5	-0.193271	2.4479167	IGF1-binding protein
Ralgps1	Ral GEF with PH domain and SH3 binding motif 1	-0.279428	2.2000685	Ral (small G protein) activator
Rbm45	RNA Binding Motif Protein 45	-0.229478	1.930666	unknown
Cml2	N-Acetyltransferase 8B	-0.189677	1.8547943	Related to chronic kidney disease
Ctcfl	CCCTC-binding factor (zinc finger protein)-like	-0.174045	1.8381633	Related to hepatocarcinoma?
Ccdc105	coiled-coil domain containing 105	-0.190840	1.7932137	Related to hepatocarcinoma?
Zfp275	zinc finger protein 275	-0.192566	1.7508389	unknown
AI429214	Chromosome 8 Open Reading Frame 48	-0.212012	1.6010274	unknown
Klhdc1	Kelch Domain Containing 1	-0.155183	1.5684341	Related to hepatic redox regulation

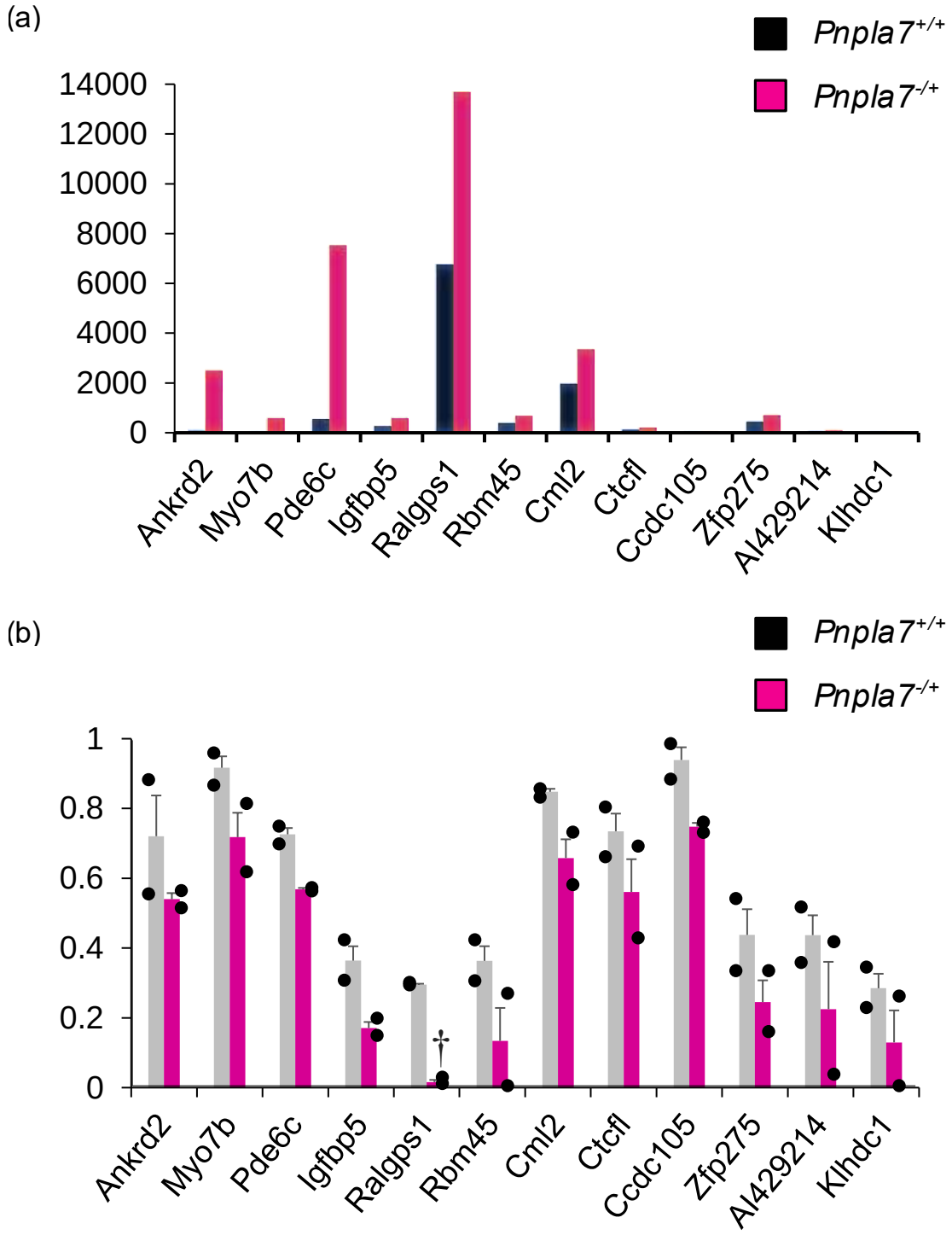

Figure 12. Graphs of the top 12 genes upregulated in the DNA methylation and downregulated in microarray analyses in the liver of *Pnpla7*$^{-/-}$ (KO) mice relative to *Pnpla7*$^{+/+}$ (WT) mice (Table 3). (a) Expression levels of the 12 genes upregulated in KO mice relative to WT mice as assessed by microarray analysis (a pool of 4 mice for each genotype). (b) Average methylation levels of the 12 genes (decreased in KO relative to WT) as assessed by RRBS analysis (n = 2, mean ± SD).

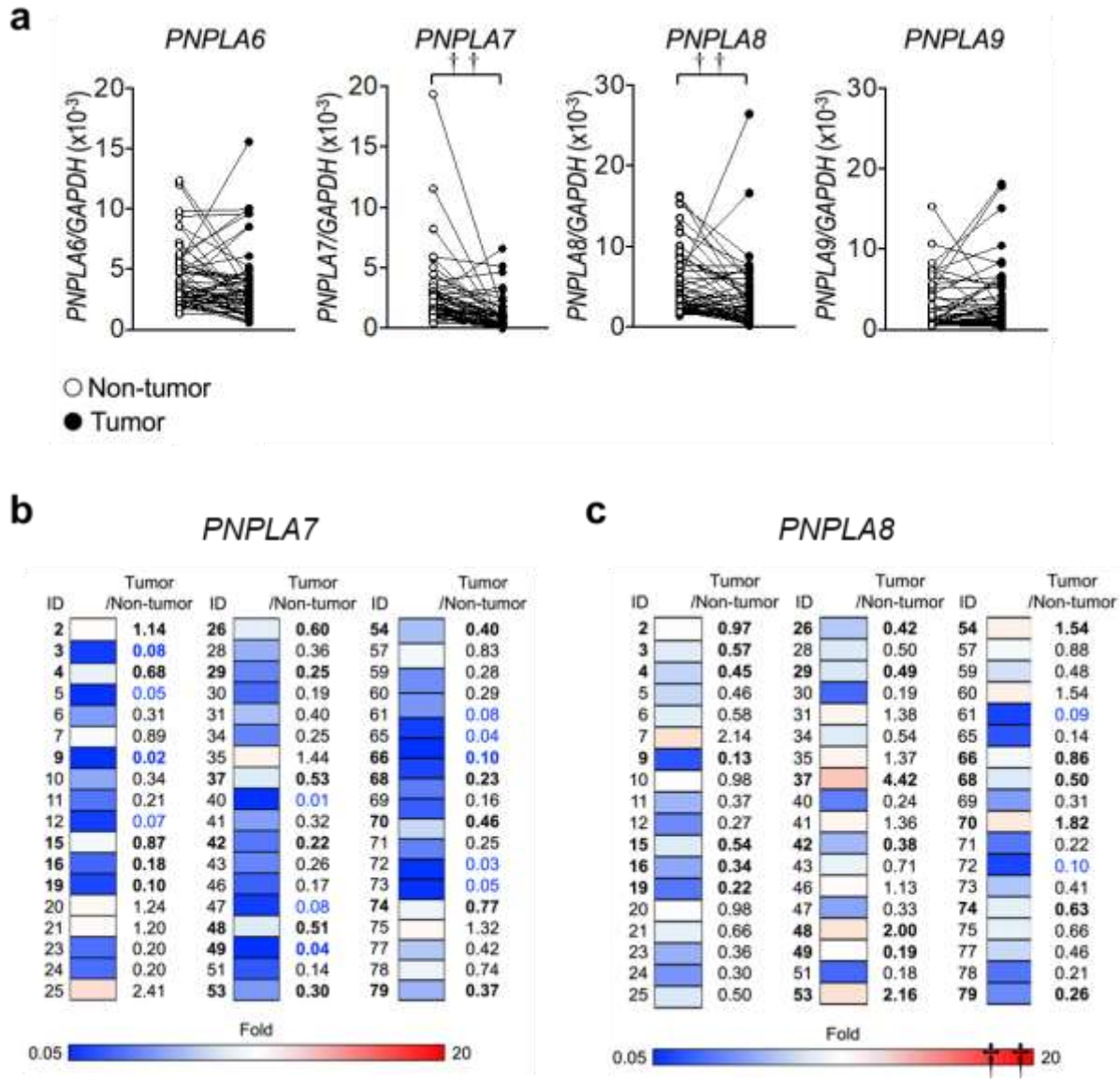

Figure 13. Expression of *PNPLA6-9* in human hepatocellular carcinoma. (a) qPCR of *PNPLA6-9* in tumor and non-tumor (n = 54 for each) tissues from human hepatocellular carcinoma patients. **, $P < 0.01$. (b, c) Heat map representation of *PNPLA7* (b) and *PNPLA8* (c) expression in individual patients. Sample IDs and expression ratios (tumor *versus* non-tumor) are indicated. Samples with marked reduction in the tumor are highlighted in blue.

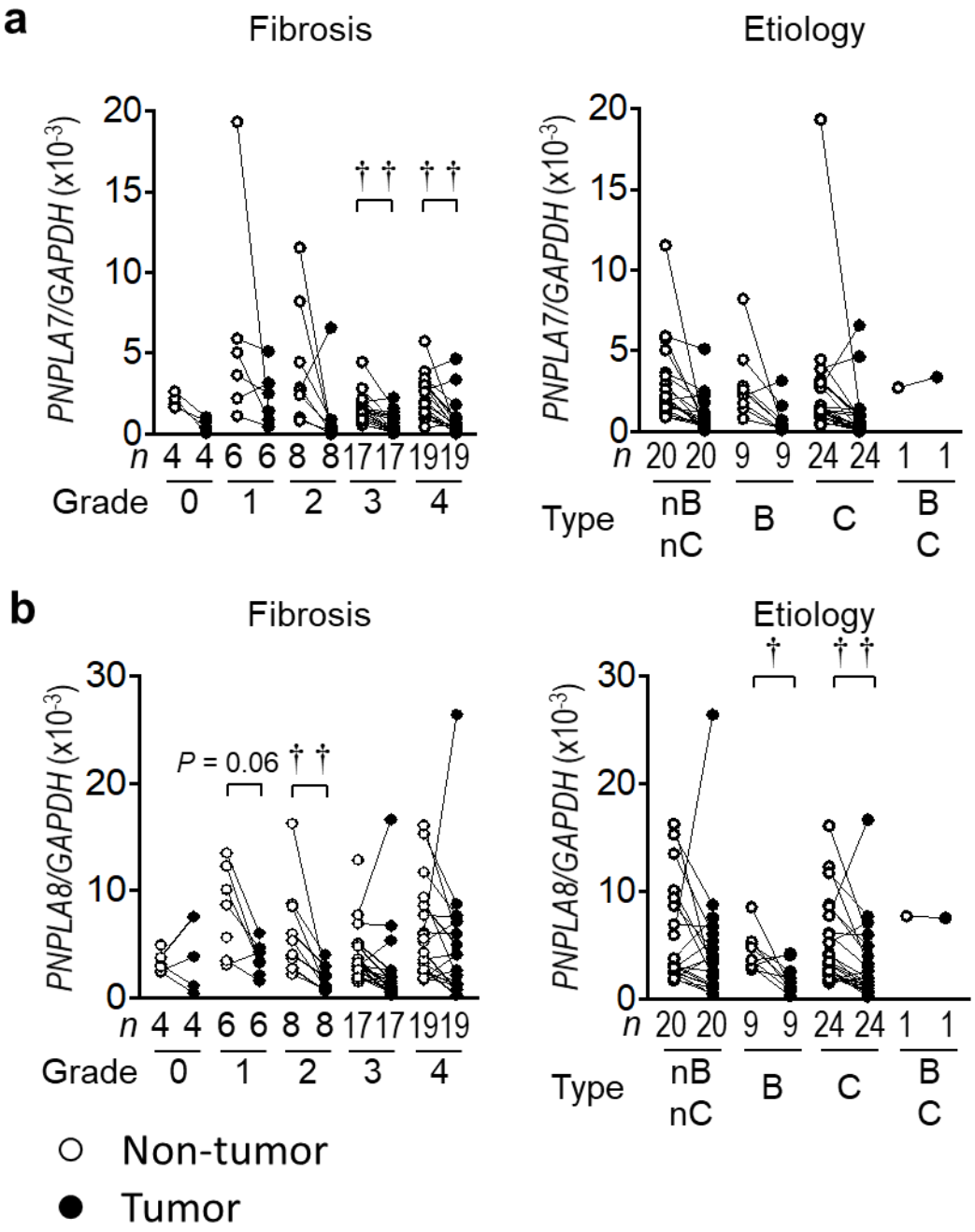

Figure 14. Expression of *PNPLA7* (a) and *PNPLA8* (b) in human hepatocellular carcinoma with different stages of fibrosis and etiology. In ethiology, nB/nC (non-B and non-C), B, C and B/C indicate HCC independent of HBV and HCV infection, that caused by HBV infection, that caused by HCV infection, and that caused by both HBV and HCV infection, respectively. *, $P < 0.05$; **, $P < 0.01$.

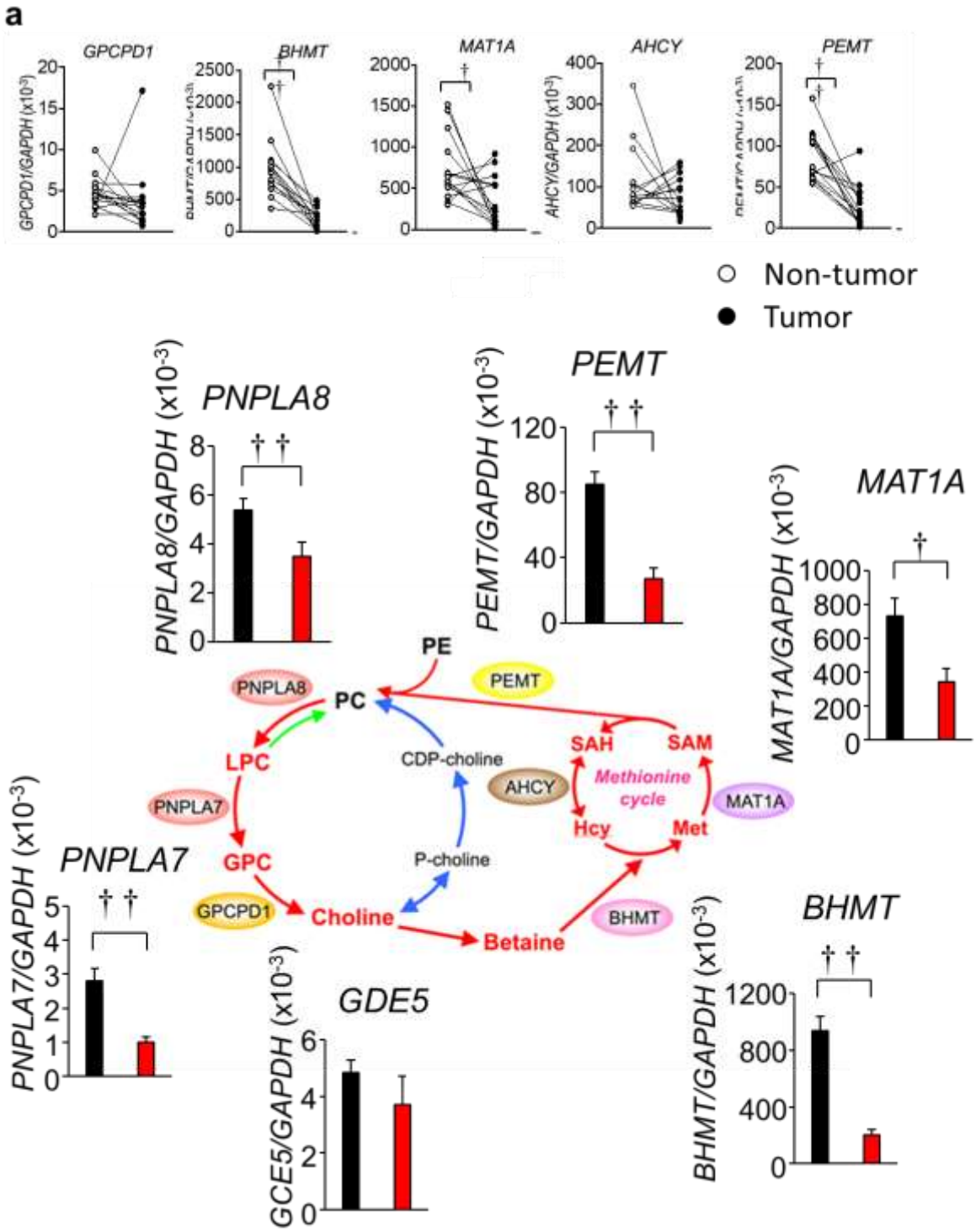

Figure 15. Expression of a series of enzymes related to the PC metabolism and methionine cycle in human hepatocellular carcinoma. (a) qPCR of *GPCPD1*, *BHMT*, *MAT1A*, *PEMT* (n = 15) and AHCY (n = 14) in tumor and non-tumor tissues from human hepatocellular carcinoma patients. (b) A schematic illustration of the PC-metabolic and methionine cycle pathways. Expression levels of the key enzymes in tumor and non-tumor tissues of human hepatocellular carcinoma are indicated. Data, mean ± SEM; *, $P < 0.05$; **, $P < 0.01$.

Discussion

Although several lipid hydrolases have the ability to exhibit lysophospholipase activity at least *in vitro* (Law et al., 2019), the molecular entity and biological roles of lysophospholipase(s) *in vivo* had remained obscure. Recently, by using a gene targeting strategy of various enzymes in the PLA_2 family, our laboratory has obtained several lines of evidence that PNPLA7, a fasting-inducible lipid hydrolase preferentially expressed in metabolically active tissues, acts as a genuine lysophospholipase that hydrolyzes LPC both *in vitro* and *in vivo* (see Introduction). Most importantly, PNPLA7 has a crucial role in metabolic homeostasis in the liver by supplying GPC, a LPC-hydrolyzed product, and thereby endogenous choline as a source of methyl groups, which are then utilized to fuel the methionine cycle. *Pnpla7* deficiency leads to substantial reduction in the hepatic levels of GPC, choline, betaine, methionine and SAM. In addition, some PC molecular species, especially those with unsaturated fatty acids, were noticeably reduced, with slight changes in PE molecular species, by *Pnpla7* deficiency. The phenotypes observed in *Pnpla7*$^{-/-}$ mice, including growth delay, kyphosis, reduced triglyceride secretion, hypoglycemia, increased energy expenditure, and decreased fat mass with adipocyte browning (Hirabayashi et al, manuscript in preparation), are similar even if not identical to those observed in mice with dietary methionine (rather than choline) insufficiency (Ables et al., 2012; Barcena et al., 2018; Parkhitko et al., 2019) or mice null for BHMT, an enzyme that catalyzes the transfer of a methyl group from betaine (a choline metabolite) to homocysteine to regenerate methionine (Teng et al., 2012). These observations

strongly suggest that the primary cause of the phenotypes in *Pnpla7*$^{-/-}$ mice could be in large part attributed to methionine shortage due to the reduced mobilization of endogenous GPC and thereby choline from membrane PC via LPC.

However, the following points still remained to be unsolved. First, although PNPLA7 expression is upregulated in the liver during fasting, it is unclear how and which nutritional component regulates this process. Second, although comprehensive metabolome analysis of the liver of *Pnpla7*$^{-/-}$ mice in comparison with *Pnpla7*$^{+/+}$ mice revealed the causal association of the PNPLA7-dependent mobilization of endogenous choline from membrane PC with the methionine cycle, and although there are many studies demonstrating the role of SAM in epigenetic modification of gene expression (Frau et al., 2012; Lu and Mato, 2012; Wang et al., 2017b; Wang et al., 2019), it remained unknown whether the PNPLA7-dependent SAM production could be linked to epigenetic regulation of gene expression through histone and/or DNA methylation. Third, although several studies have demonstrated close associations of gene mutations in the PNPLA family with human diseases (Fischer et al., 2007; Hirabayashi et al., 2017; Kmoch et al., 2015; Morgan et al., 2006; Romeo et al., 2008; Saunders et al., 2015), the relationship of PNPLA7 with human liver diseases was poorly understood. The present study has addressed these questions to gain new insights into the regulatory roles of PNPLA7 in homeostasis and disease.

Methionine availability controls PNPLA7 expression

It is known that the expressions and/or functions of metabolic enzymes (*e.g*. those involved in glycolysis, TCA cycle, and nucleotide biosynthesis) are often regulated by their own metabolites as a feedback mechanism to maintain optimal metabolic flow and to avoid futile cycles. Herein, we have demonstrated using a HepG2 hepatocellular carcinoma cell line as a model that PNPLA7 expression is controlled by its downstream metabolite, namely methionine (rather than choline), being upregulated in the absence of methionine and downregulated in its presence. Because of high demand of exogenous methionine in liver cells, culture of the cells in methionine-free medium led to marked reduction in the intracellular pool of methionine and thereby various methionine-derived metabolites such as SAM among others. The reduced flux from SAM to SAH, mirroring the reduced transmethylation reaction, in methionine-free culture can be further supported, for instance, by a marked decrease of sarcosine (a methylation product of glycine), whose biosynthesis is highly coupled with SAM to SAH conversion by GNMT (Luka et al., 2009; Sreekumar et al., 2009). Importantly, the decreases in multiple methionine/SAM-related metabolites, along with the changes in many other metabolites directly or indirectly associated with the methionine cycle, such as transsulfuration, polyamine metabolism, urea cycle, nucleotide synthesis, glycolysis, and TCA cycle (Figures 6), are largely even if not solely recapitulated in the liver of *Pnpla7*$^{-/-}$ mice,

providing further evidence that PNPLA7-driven phospholipid catabolism is functionally linked to methionine metabolism.

Serine, which is produced by the *de novo* synthesis from glucose and exogenous uptake, supports the methionine cycle through *de novo* ATP synthesis to allow the conversion of methionine to SAM, and contributes to purine synthesis via serine-derived one carbon units (Maddocks et al., 2016). Impaired glycine-serine conversion may explain that serine-derived one carbons, in the form of methyl group, to the folate cycle is a predominant flux over glycine-serine conversion. Serine-derived one carbon metabolism supports NADPH production by oxidation of methylene THF to 10-formyl-THF, which corresponds to reduction of $NADP^+$ to NADPH (Fan et al., 2014; Maddocks et al., 2016; Snell et al., 1987). Although metabolites in the oxidative pentose phosphate pathway, which is the main route to produce NADPH from glucose (Fan et al., 2014), are not significantly changed (data are not shown), NADPH accumulates, while $NADP^+$, an oxidative form of NADPH, is dramatically reduced, in methionine-depleted cells (Figure 6(h)). Because two molecules of NADPH are consumed to synthesize each molecule of acetate, which is sequentially incorporated into long-chain fatty acids by fatty acid synthase, this result indicates that fatty acid synthesis is likely blocked when methionine is not available (Salati et al., 1996). According to the reduction of SAM, the flux from putrescine to spermine in the polyamine pathway are disturbed, causing the increase of

putrescine and spermidine and the reduction of spermine (Figure 6(c)), which may perturb cell differentiation and proliferation (Wang et al., 2017a).

It is notable that several choline metabolites, including GPC, choline, phosphocholine and CDP-choline, are elevated in cells cultured in methionine-free medium (Figure 6(d)). This event could be explained, at least partly, by robust upregulation of PNPLA7, which supplies GPC from LPC. It is tempting to speculate that the induction of PNPLA7 after methionine depletion (and probably after fasting *in vivo*) may reflect a sort of metabolic adaptations to compensate for the insufficient availability of methyl groups. Additionally, the striking increase of choline, phosphocholine and CDP-choline, relative to GPC, in methionine-depleted cells may be indicative of an increased uptake of exogenous choline through choline transporters. Nonetheless, the increased flux from choline to CDP-choline in methionine-depleted cells implies that PC biosynthesis through the Kennedy pathway is accelerated to maintain cell membrane homeostasis, in agreement with the view that the impairment of the PEMT pathway leads to compensatory upregulation of the Kennedy pathway for *de novo* PC biosynthesis (Li et al., 2005; Li and Vance, 2008; van der Veen et al., 2017; Vance, 2013). Effects of methionine restriction on lipid metabolism in mice were previously reported in several studies. For instance, progeroid mice fed a methionine-restricted diet showed the recovery of some lipid-metabolic pathways including biosynthesis of unsaturated fatty acids and glycerophospholipid metabolism, with restoration of several polyunsaturated and monounsaturated fatty acids to the

levels similar to those in WT mice (Bárcena et al., 2018). Further, livers from rats fed a methionine-restricted diet showed the reduction of the expression levels of genes and proteins involved in the synthesis of triglycerides, cholesterol and phospholipids, along with decreased fatty acid synthesis and enhanced fatty acid oxidation (Malloy et al., 2013). These notions can support the results in this study.

The methylation rate in the promoter region of HepG2 cells is extraordinarily higher than normal liver cells, and after treating HepG2 cells with a DNA methyltransferase inhibitor, the expression level of *PNPLA7* was upregulated following demethylation of its promoter (Zhang et al., 2016). Our results indicate that the methylation level of the *PNPLA7* promoter is reduced to about 60% in methionine-deficient cells in which SAM is nearly absent, suggesting that the reduction of SAM-dependent methylation of the *PNPLA7* promoter eventually allows for upregulation of its expression. When methionine deficiency dampens the flow of methionine cycle, choline cycle may substitute PC synthesis to maintain PC level, in which PNPLA7 may play a role as a rate-liming enzyme, leading to upregulation of PNPLA7 expression. Although the molecular mechanism whereby PNPLA7, but not other PNPLA enzymes, is induced by methionine insufficiency is currently unknown, certain transcription factors or specific histone modifications that can be sensitive to methionine availability might specifically regulate the expression of PNPLA7. Recently, several studies have focused on the relationship between lipid metabolism and DNA methylation in the field of lipid-related

diseases (Hedman et al., 2017; Mittelstrass and Waldenberger, 2018; Zhong et al., 2016), although the underlying molecular mechanisms remain largely unexplored. As SAM appears to be associated with DNA and/or histone methylation to regulate the expression of various genes including *PNPLA7*, SAM can be a key component to explain the molecular mechanism for interconnection between lipids and epigenome. Although a transcription factor responsible for the induction of *PNPLA7* expression remains to be determined, searching the database ChIP-Atlas for transcription factors activated by fasting revealed that FOXO1 is a potential candidate that binds to the promoter region of the *PNPLA7* gene. The transcriptional activity of FOXO is suppressed through phosphorylation by AKT downstream of insulin signal, whereas it is activated through JNK and AMPK under hypotrophic conditions where the insulin signal is attenuated (Hay, 2011; Matsumoto et al., 2007). In support of this idea, PNPLA7 expression in adipocytes is downregulated by insulin (Kienesberger et al., 2008).

Taken together, the present study highlights a new mechanism underlying the nutritional regulation of PNPLA7 expression. In a methionine-rich environment, PNPLA7 expression is downregulated through hypermethylation of the *PNPLA7* promoter. Methionine depletion decreases intracellular SAM level and thereby SAM-dependent methylation of the *PNPLA7* promoter, enabling the upregulation of its gene expression. The increased PNPLA7 replenishes GPC and choline through breakdown of LPC, which is derived from membrane PC. This endogenous choline pool is then used for supply of methyl groups to the methionine cycle

to overcome methionine insufficiency, and also for *de novo* PC synthesis through the Kennedy pathway to maintain membrane homeostasis.

PNPLA7-driven SAM is coupled with epigenetic regulation

In this study, global histone methylation analysis, genome-wide DNA methylation analysis, and microarray gene profiling using livers from *Pnpla7*$^{-/-}$ and *Pnpla7*$^{+/+}$ mice revealed that PNPLA7-driven SAM production is likely coupled with methylation of histones and gene promoters that could affect gene expression. To gain further evidence, however, it would be important to examine whether the decreased histone and/or DNA methylation in *Pnpla7*$^{-/-}$ mice could be rescued by supplementation with exogenous methionine or SAM in a future study. Although an attempt to knockdown *PNPLA7* in HepG2 cells was unsuccessful in this study because its low basal expression and the knockdown efficiency was only partial, primary hepatocytes obtained from *Pnpla7*$^{-/-}$ mice displayed multiple phenotypes reminiscent of methionine insufficiency as previously reported, which were rescued by supplementation with excess methionine in culture media, implying that the phenotypes in *Pnpla7* deficiency could be explained in large part by methionine shortage (Hirabayashi et al, manuscript in preparation). Accordingly, metabolites in hepatocytes from *Pnpla7*$^{+/+}$ mice fed with a methionine-deficient diet would show the similar responses with those observed in *Pnpla7*$^{-/-}$ mice. Although the effects of *Pnpla7* deficiency on histone and DNA methylation are not so dramatic, with only

modest changes in the methylation of limited members of histones and genes, this study is, to our knowledge, the first demonstration that phospholipid catabolism by a member of the PLA_2 family is linked to epigenetic control of gene expression *in vivo*.

Among the histones, methylation of H3:K79 is affected rather specifically by *Pnpla7* deficiency. Methylation of H3:K79, which is mediated by the histone methyltransferase Dot1/Dot1L, is involved in the regulation of telomeric silencing, cellular development, cell-cycle checkpoint, DNA repair, and regulation of transcription, and appears to have a crucial role in oncogenic transformation as well as disease progression in leukemia involving several oncogenic fusion proteins (Farooq et al., 2016). Considering that *Pnpla7* deficiency reduces H3:K79 methylation and that Dot1/Dot1L-mediated H3:K79 methylation generally enhances the transcription of target genes, this histone modification may be involved in the expression of some genes that are decreased in *Pnpla7*$^{-/-}$ mice relative to *Pnpla7*$^{+/+}$ mice.

Genome-wide DNA methylation analysis, in combination with microarray gene profiling, revealed that, of nearly 20,000 genes, 12 genes showed significantly lower promoter methylation and higher gene expression in *Pnpla7*$^{-/-}$ mice than in *Pnpla7*$^{+/+}$ mice, suggesting that PNPLA7-driven SAM production is linked to the epigenetic regulation of their expressions. These genes include those potentially implicated in hepatic fibrosis, growth, signal transduction, oncogenic transformation, and redox regulation. Indeed, upregulation of *Ankrd2* and *Myo7b*, which have been implicated in muscle development (Cenni et al., 2011; Mohamed et al., 2013),

might be related to the fact that choline/methionine deficiency is associated with NAFLD and NASH (de Wit et al., 2012; Farrell et al., 2019), and that of *Igfbp5*, which counteracts IGF-1 (Weng et al., 2019), might account for growth retardation of *Pnpla7*$^{-/-}$ mice. Moreover, the expression of some of these genes has been shown to undergo epigenetic control of their expression (Salgado-Albarran et al., 2019; Xu et al., 2018). Presumably, knockout of *Pnpla7* might be linked to the removal of methyl groups from the promoter regions of these 12 genes, leading to their upregulation. Although the precise association of the epigenetic alterations with various phenotypes of *Pnpla7*$^{-/-}$ mice is still largely unclear, our study nonetheless provides the first clue of evidence that phospholipid catabolism is functionally linked to epigenetic regulation of gene expression. Although the observed changes in several if not all metabolites in *Pnpla7*$^{-/-}$ mice might have occurred indirectly rather than directly, the changes in most metabolites and associated gene expression were already evident at an earlier stage (4-week old), a timing of weaning when growth retardation began (data not shown), supporting the conclusion that the metabolic changes in the null mice are associated with epigenetic alterations.

PNPLA7 and liver cancer in humans

It has currently been reported that SAM can provide either positive or negative effect on cancer development depending on the types of cancer. In particular, SAM stimulates the growth

of cancer stem cells as well as colorectal and prostate cancers (Gao et al., 2019; Wang et al., 2019), whereas it prevents the development of liver cancer (Pascale et al., 1992; Wang et al., 2017b). In this study, we have shown that the expression of *PNPLA7*, as well as several other enzymes involved in the PC catabolism and methionine cycle, was markedly decreased in clinical specimens of human hepatocellular carcinoma, regardless of the states of fibrosis and etiology. The possibility is that the ratio of stroma cells to cancer cells is increased in hepatocellular carcinoma is unlikely, since the expression of PNPLA6 and PNPLA9 were unchanged in the tumor regions (Figure 13(a)). These observations, together with previous studies showing the decreased expression of BHMT (which transfers a methyl group to homocysteine to give rise to methionine) and MAT1A (which converts methionine to SAM) in hepatocellular carcinoma (Jin et al., 2016; Mato et al., 2002), imply that the endogenous flux of SAM through the PC-catabolic pathway and methionine cycle is declined in hepatocellular carcinoma, consistent with the view that the decreased SAM level is associated with liver cancer development. Although the decreased expression of *PNPLA7* in human hepatocellular carcinoma is due, at least in part, to hypermethylation in the promoter region of *PNPLA7* (Zhang et al., 2016), this appears to be inconsistent with the view that the decreased SAM level should reduce DNA methylation in general. Because cancer stem cells have high SAM flux (Gao et al., 2019; Wang et al., 2019), we speculate that the hypermethylation of the *PNPLA7* promoter may already occur in cancer stem cell and be sustained even in the developed stages

of liver cancer. In another word, hypermethylation of the PNPLA7 promoter is likely to be a main cause of downregulation of PNPLA7 expression. Considering that PNPLA7 expression is downregulated by insulin (Heier et al., 2017) and insulin signaling is constitutively activated in hepatocellular carcinoma (Sakurai et al., 2017), activated insulin signaling in liver cancer may cause downregulation of PNPLA7 expression. PNPLA8, the upstream component in the PC-catabolic pathway, may also undergo similar epigenetic regulation, although this possibility needs further investigation. Alternatively, downregulation of PNPLA8 in hepatocellular carcinoma might be due to the inactivation of SREBP-2, because PNPLA8 expression is regulated by SREBP-2 binding to the PNPLA8 promoter (Kim et al., 2016).

A growing body of evidence suggests that SAM inhibits the growth, transformation, and invasion of liver cancer (Frau et al., 2012; Wang et al., 2017b). SAM deficiency strongly favors hepatocellular carcinoma development, which can be inhibited by exogenous supply of SAM (Lozano-Rosas et al., 2020; Pascale et al., 1992). Low SAM and high SAH levels, indicative of high methylation activity and liver injury sensitivity, are characteristics of the development of hepatocellular carcinoma (Pascale et al., 2018). SAM supplementation in *Mdr2*-deficient mice, a model of inflammation-associated hepatocellular carcinoma, inhibits liver tumor development potentially by increasing multiple tumor suppressor mechanisms resulting in cell cycle arrest (Stoyanov et al., 2017). *Mat1a*-deficient mice, which display hepatic SAM deficiency, are highly susceptible to development of liver cancer (Lu et al., 2001; Martinez-Chantar et al.,

2002). SAM treatment increases the expression of DUSP1, a dual phosphatase that blocks growth-promoting ERK signaling, thus reducing malignant degeneration (Tomasi et al., 2010). Methylome analysis using bisulfite mapping capturing promoters and enhancers revealed that SAM globally alters the methylation landscape and thereby downregulates a set of genes required for cellular transformation and invasiveness of liver cancer cells (Wang et al., 2017b). These studies have provided a rationale for SAM as an anti-cancer agent against hepatocellular carcinoma.

On the other hand, the promoting effect of SAM on the growth of cancer stem cells and other types of cancer may be related to the recently emerging concept that methionine restriction extends lifespan (Ables et al., 2016). Reportedly, methionine restriction exerts beneficial effects on metabolic health and inflammatory responses by improving glucose metabolism, protecting against obesity and hepatic steatosis, attenuating growth, and reducing oxidative stress (Ables et al., 2012; Barcena et al., 2018; Parkhitko et al., 2019). Stimulating SAM synthesis extends lifespan via activation of AMPK (Ogawa et al., 2016). Not surprisingly, methionine restriction has been implicated in delaying the progression of cancer. Indeed, methionine restriction reduces the formation of colon cancer (Komninou et al., 2006) and prostate cancer (Sinha et al., 2014), and has a therapeutic effect on chemotherapy-resistant colorectal cancer (Gao et al., 2019). Some cancers show the absolute requirement for nutritional supply of methionine, a phenomenon known as ‘methionine dependence’ (Cellarier et al., 2003).

Cancer stem cells, with a marked dependence on exogenous methionine, exhibit a high methionine cycle flux and contain abundant methionine metabolites, and accordingly, pharmacological inhibition or genetic manipulation of the methionine cycle is sufficient to prevent the tumor-forming capacity due to depletion of SAM (Wang et al., 2019). SAM is the most elevated metabolite in human colorectal cancer compared with the non-tumor tissue (Satoh et al., 2017). Moreover, an increased flux into the transsulfuration pathway, which is coupled with SAM to SAH conversion in the methionine cycle, is crucial for the promotion of tumor growth by increasing the synthesis of glutathione, an anti-oxidant metabolite (Zhu et al., 2019). Overall, the promoting *versus* inhibitory effects of SAM on cellular proliferation are cell-type specific, and the latter effect appears to be dominant in the case of hepatocellular carcinoma (Lu and Mato, 2012).

The molecular mechanism whereby multiple enzymes in the metabolic pathway through the PC catabolism and methionine cycle are simultaneously downregulated in liver cancer is currently unknown. Considering that hepatocellular carcinoma (like HepG2 cells) exhibits a high dependence on exogenous methionine, high metabolic flux of exogenous methionine in association with SAM-dependent methylation might eventually lead to shutting off the flux of endogenous methionine by downregulating key metabolic enzymes as a negative-feedback mechanism. In support of this notion, CpG island in the *PNPLA7* promoter is hypermethylated in several human hepatocellular carcinoma cell lines (Zhang et al., 2016), and methionine

depletion reduces this methylation state to relieve *PNPLA7* transcription, as shown in this study. Similarly, epigenetic methylation of the *MAT1A* promoter leads to downregulation of its expression (Frau et al., 2012). Behind the epigenetic regulation, it is possible that a common transcription factor(s) might be responsible for the simultaneous expression of these genes.

Taken together, concomitant reduction of a series of enzymes involved in the PC catabolism and methionine cycle, particularly *PNPLA7* whose expression level is dramatically attenuated in most hepatocellular carcinoma patients, could be a novel diagnostic marker of this life-threatening disease. Furthermore, controlling SAM levels by manipulating the expression or activity of PNPLA7 would be a novel therapeutic strategy for treatment of liver cancer and possibly other cancers.

Future prospects

This study has identified that exogenous methionine controls the expression of PNPLA7 and demonstrated the interconnection between PNPLA7, acting as a lysophospholipase, and epigenome. However, further investigations are needed to confirm these observations. First, the association of PNPLA7 with methionine metabolism should be verified if the levels of metabolites in the choline/methionine cycle and the rate of DNA methylation are concomitantly decreased when HepG2 cells with PNPLA7 depletion is cultured in methionine-depleted medium. Second, *in vitro* and *in vivo* findings can be linked if the rate of DNA methylation of

the same genes or functionally similar genes that are downregulated *in vivo* would be also downregulated in PNPLA7-silenced HepG2 cells. Third, the *in vitro* and *in vivo* findings can be connected more positively if the levels of metabolites in the choline/methionine cycle show similar changes, expression level of *Pnpla7* is upregulated, and the promoter region of *Pnpla7* is demethylated when WT mice are fed with a methionine-deficient diet. Fourth, as previously described, the relationship between PNPLA7 and epigenome via SAM can be more positively suggested if the expression levels of particular genes that were downregulated in the liver of *Pnpla7*$^{-/-}$ mice, and also the overall phenotypes observed in *Pnpla7*$^{-/-}$ mice, could be rescued by supplementation with excessive SAM. Fifth, the relationship between PNPLA7 and human hepatocellular carcinoma can be more affirmed if the rate of DNA methylation in the promoter region of PNPLA7 in tumor regions would be increased in comparison with that in non-tumor regions of the liver.

Conclusion

Our previous study demonstrated that PNPLA7 works as a fasting-inducible lysophopholipase that hydrolyzes LPC to produce choline via GPC in the liver. Metabolome analysis of liver in *Pnpla7*-deficient mice revealed that metabolites in the choline/methionine cycle, such as GPC, choline, betaine, methionine and SAM, are decreased, highlighting the role of PNPLA7 as a checkpoint of the endogenous methyl group flux from hydrophobic PC to hydrophilic metabolites in the methionine cycle. Given this background, my research has explored the underlying functions of PNPLA7 in three perspectives. First, the expression level of PNPLA7 is controlled by the availability of methionine. Decreased methylation in the promoter region of PNPLA7 in human hepatocellular carcinoma cells under methionine-deficient condition leads to upregulation of PNPLA7, which may be relevant to its upregulation during fasting *in vivo*. Second, PNPLA7 may contribute to the changes of epigenetic modifications for histones and DNA through regulating the availability of SAM. Third, the expression levels of PNPLA7 and related enzymes in the choline/methionine cycle are decreased in clinical specimens of human hepatocellular carcinoma. We speculate that high metabolic flux of exogenous methionine in association with SAM-dependent methylation might eventually lead to shutting off the flux of endogenous methionine by downregulating key metabolic enzymes as a negative-feedback mechanism. Taken altogether, my research has revealed that PNPLA7 is a lipolytic enzyme that links phospholipids to epigenetic regulation. This research offers a new platform in the fields of lipid and epigenome biology.

References

Santos, A., Parrini, M.C., and Camonis, J. (2016). RalGPS2 is essential for survival and cell cycle progression of lung cancer cells independently of its established substrates Ral GTPases. PLoS One *11*, e0154840.

Abbasi, I.H.R., Abbasi, F., Soomro, R.N., Abd El-Hack, M.E., Abdel-Latif, M.A., Li, W., Hao, R., Sun, F., Bodinga, B.M., Hayat, K.*, et al.* (2017). Considering choline as methionine precursor, lipoproteins transporter, hepatic promoter and antioxidant agent in dairy cows. AMB Express *7*, 214.

Ables, G.P., Hens, J.R., and Nichenametla, S.N. (2016). Methionine restriction beyond life-span extension. Ann N Y Acad Sci *1363*, 68-79.

Ables, G.P., Perrone, C.E., Orentreich, D., and Orentreich, N. (2012). Methionine-restricted C57BL/6J mice are resistant to diet-induced obesity and insulin resistance but have low bone density. PLoS One *7*, e51357.

Aiba, T., Saito, T., Hayashi, A., Sato, S., Yunokawa, H., Fukami, M., Hayashi, Y., Mizuno, K., Sato, Y., Kojima, Y.*, et al.* (2019). Exploring disease-specific methylated CpGs in human male genital abnormalities by using methylated-site display-amplified fragment length polymorphism (MSD-AFLP). J Reprod Dev *65*, 491-497.

Aiba, T., Saito, T., Hayashi, A., Sato, S., Yunokawa, H., Maruyama, T., Fujibuchi, W., Kurita, H., Tohyama, C., and Ohsako, S. (2017). Methylated site display (MSD)-AFLP, a sensitive and affordable method for analysis of CpG methylation profiles. BMC Mol Biol *18*, 7.

Banco, M.T., Mishra, V., Greeley, S.C., and Ronning, D.R. (2018). Direct detection of products from *S*-Adenosylmethionine-dependent enzymes using a competitive fluorescence polarization assay. Anal Chem *90*, 1740-1747.

Barcena, C., Quiros, P.M., Durand, S., Mayoral, P., Rodriguez, F., Caravia, X.M., Marino, G., Garabaya, C., Fernandez-Garcia, M.T., Kroemer, G.*, et al.* (2018). Methionine restriction extends lifespan in progeroid mice and alters lipid and bile acid metabolism. Cell Rep *24*, 2392-2403.

Bjorkoy, G., Overvatn, A., Diaz-Meco, M.T., Moscat, J., and Johansen, T. (1995). Evidence for a bifurcation of the mitogenic signaling pathway activated by Ras and phosphatidylcholine-hydrolyzing phospholipase C. J Biol Chem *270*, 21299-21306.

Bligh, E.G., and Dyer, W.J. (1959). A rapid method of total lipid extraction and purification. Can J Biochem Physiol *37*, 911-917.

Bock, C., Tomazou, E.M., Brinkman, A.B., Muller, F., Simmer, F., Gu, H., Jager, N., Gnirke, A., Stunnenberg, H.G., and Meissner, A. (2010). Quantitative comparison of genome-wide DNA methylation mapping technologies. Nat Biotechnol *28*, 1106-1114.

Bonora, G., Rubbi, L., Morselli, M., Ma, F., Chronis, C., Plath, K., and Pellegrini, M. (2019). DNA methylation estimation using methylation-sensitive restriction enzyme bisulfite sequencing (MREBS). PLoS One *14*, e0214368.

Cano, A., Buque, X., Martinez-Una, M., Aurrekoetxea, I., Menor, A., Garcia-Rodriguez, J.L.,

Lu, S.C., Martinez-Chantar, M.L., Mato, J.M., Ochoa, B., *et al.* (2011). Methionine adenosyltransferase 1A gene deletion disrupts hepatic very low-density lipoprotein assembly in mice. Hepatology *54*, 1975-1986.

Castellano, R., Perruchot, M.H., Conde-Aguilera, J.A., van Milgen, J., Collin, A., Tesseraud, S., Mercier, Y., and Gondret, F. (2015). A methionine deficient diet enhances adipose tissue lipid metabolism and alters anti-oxidant pathways in young growing pigs. PLoS One *10*, e0130514.

Cellarier, E., Durando, X., Vasson, M.P., Farges, M.C., Demiden, A., Maurizis, J.C., Madelmont, J.C., and Chollet, P. (2003). Methionine dependency and cancer treatment. Cancer Treat Rev *29*, 489-499.

Cenni, V., Bavelloni, A., Beretti, F., Tagliavini, F., Manzoli, L., Lattanzi, G., Maraldi, N.M., Cocco, L., and Marmiroli, S. (2011). Ankrd2/ARPP is a novel Akt2 specific substrate and regulates myogenic differentiation upon cellular exposure to H_2O_2. Mol Biol Cell *22*, 2946-2956.

Chin, K.T., Xu, H.T., Ching, Y.P., and Jin, D.Y. (2007). Differential subcellular localization and activity of kelch repeat proteins KLHDC1 and KLHDC2. Mol Cell Biochem *296*, 109-119.

da Costa, K.A., Badea, M., Fischer, L.M., and Zeisel, S.H. (2004). Elevated serum creatine phosphokinase in choline-deficient humans: mechanistic studies in C2C12 mouse myoblasts. Am J Clin Nutr *80*, 163-170.

da Costa, K.A., Niculescu, M.D., Craciunescu, C.N., Fischer, L.M., and Zeisel, S.H. (2006). Choline deficiency increases lymphocyte apoptosis and DNA damage in humans. Am J Clin Nutr *84*, 88-94.

de Wit, N.J., Afman, L.A., Mensink, M., and Muller, M. (2012). Phenotyping the effect of diet on non-alcoholic fatty liver disease. J Hepatol *57*, 1370-1373.

Delgado-Reyes, C.V., Wallig, M.A., and Garrow, T.A. (2001). Immunohistochemical detection of betaine-homocysteine *S*-methyltransferase in human, pig, and rat liver and kidney. Arch Biochem Biophys *393*, 184-186.

Ducker, G.S., and Rabinowitz, J.D. (2017). One-carbon metabolism in health and disease. Cell Metab *25*, 27-42.

Eisenberg, T., Abdellatif, M., Schroeder, S., Primessnig, U., Stekovic, S., Pendl, T., Harger, A., Schipke, J., Zimmermann, A., Schmidt, A.*, et al.* (2016). Cardioprotection and lifespan extension by the natural polyamine spermidine. Nat Med *22*, 1428-1438.

Enooku, K., Uranbileg, B., Ikeda, H., Kurano, M., Sato, M., Kudo, H., Maki, H., Koike, K., Hasegawa, K., Kokudo, N.*, et al.* (2016). Higher LPA2 and LPA6 mRNA Levels in Hepatocellular Carcinoma Are Associated with Poorer Differentiation, Microvascular Invasion and Earlier Recurrence with Higher Serum Autotaxin Levels. PLoS One *11*, e0161825.

Fan, J., Ye, J., Kamphorst, J.J., Shlomi, T., Thompson, C.B., and Rabinowitz, J.D. (2014). Quantitative flux analysis reveals folate-dependent NADPH production. Nature *510*, 298-302.

Farooq, Z., Banday, S., Pandita, T.K., and Altaf, M. (2016). The many faces of histone H3K79 methylation. Mutat Res Rev Mutat Res *768*, 46-52.

Farrell, G., Schattenberg, J.M., Leclercq, I., Yeh, M.M., Goldin, R., Teoh, N., and Schuppan, D. (2019). Mouse models of nonalcoholic steatohepatitis: toward optimization of their relevance to human nonalcoholic steatohepatitis. Hepatology *69*, 2241-2257.

Fischer, J., Lefevre, C., Morava, E., Mussini, J.M., Laforet, P., Negre-Salvayre, A., Lathrop, M., and Salvayre, R. (2007). The gene encoding adipose triglyceride lipase (*PNPLA2*) is mutated in neutral lipid storage disease with myopathy. Nat Genet *39*, 28-30.

Frau, M., Tomasi, M.L., Simile, M.M., Demartis, M.I., Salis, F., Latte, G., Calvisi, D.F., Seddaiu, M.A., Daino, L., Feo, C.F.*, et al.* (2012). Role of transcriptional and posttranscriptional regulation of methionine adenosyltransferases in liver cancer progression. Hepatology *56*, 165-175.

Gao, X., Sanderson, S.M., Dai, Z., Reid, M.A., Cooper, D.E., Lu, M., Richie, J.P., Jr., Ciccarella, A., Calcagnotto, A., Mikhael, P.G.*, et al.* (2019). Dietary methionine influences therapy in mouse cancer models and alters human metabolism. Nature *572*, 397-401.

Gujar, H., Weisenberger, D.J., and Liang, G. (2019). The roles of human DNA methyltransferases and their isoforms in shaping the epigenome. Genes (Basel) *10*.

Harayama, T., Eto, M., Shindou, H., Kita, Y., Otsubo, E., Hishikawa, D., Ishii, S., Sakimura, K., Mishina, M., and Shimizu, T. (2014). Lysophospholipid acyltransferases mediate

phosphatidylcholine diversification to achieve the physical properties required in vivo. Cell Metab *20*, 295-305.

Harris, R.A., Wang, T., Coarfa, C., Nagarajan, R.P., Hong, C., Downey, S.L., Johnson, B.E., Fouse, S.D., Delaney, A., Zhao, Y.*, et al.* (2010). Comparison of sequencing-based methods to profile DNA methylation and identification of monoallelic epigenetic modifications. Nat Biotechnol *28*, 1097-1105.

Hasek, B.E., Boudreau, A., Shin, J., Feng, D., Hulver, M., Van, N.T., Laque, A., Stewart, L.K., Stone, K.P., Wanders, D.*, et al.* (2013). Remodeling the integration of lipid metabolism between liver and adipose tissue by dietary methionine restriction in rats. Diabetes *62*, 3362-3372.

Hay, N. (2011). Interplay between FOXO, TOR, and Akt. Biochim Biophys Acta *1813*, 1965-1970.

He, J., Huang, Y., Liu, Z., Zhao, R., Liu, Q., Wei, L., Yu, X., Li, B., and Qin, Y. (2017). Hypomethylation of BORIS is a promising prognostic biomarker in hepatocellular carcinoma. Gene *629*, 29-34.

Hedman, A.K., Mendelson, M.M., Marioni, R.E., Gustafsson, S., Joehanes, R., Irvin, M.R., Zhi, D., Sandling, J.K., Yao, C., Liu, C.*, et al.* (2017). Epigenetic Patterns in Blood Associated With Lipid Traits Predict Incident Coronary Heart Disease Events and Are Enriched for Results From Genome-Wide Association Studies. Circ Cardiovasc Genet *10*.

Heier, C., Kien, B., Huang, F., Eichmann, T.O., Xie, H., Zechner, R., and Chang, P.A. (2017).

The phospholipase PNPLA7 functions as a lysophosphatidylcholine hydrolase and interacts with lipid droplets through its catalytic domain. J Biol Chem *292*, 19087-19098.

Hirabayashi, T., Anjo, T., Kaneko, A., Senoo, Y., Shibata, A., Takama, H., Yokoyama, K., Nishito, Y., Ono, T., Taya, C.*, et al.* (2017). PNPLA1 has a crucial role in skin barrier function by directing acylceramide biosynthesis. Nat Commun *8*, 14609.

Jin, B., Gong, Z., Yang, N., Huang, Z., Zeng, S., Chen, H., Hu, S., and Pan, G. (2016). Downregulation of betaine homocysteine methyltransferase (BHMT) in hepatocellular carcinoma associates with poor prognosis. Tumour Biol *37*, 5911-5917.

Kempson, S.A., Zhou, Y., and Danbolt, N.C. (2014). The betaine/GABA transporter and betaine: roles in brain, kidney, and liver. Front Physiol *5*, 159.

Kienesberger, P.C., Lass, A., Preiss-Landl, K., Wolinski, H., Kohlwein, S.D., Zimmermann, R., and Zechner, R. (2008). Identification of an insulin-regulated lysophospholipase with homology to neuropathy target esterase. J Biol Chem *283*, 5908-5917.

Kim, K.Y., Jang, H.J., Yang, Y.R., Park, K.I., Seo, J., Shin, I.W., Jeon, T.I., Ahn, S.C., Suh, P.G., Osborne, T.F.*, et al.* (2016). SREBP-2/PNPLA8 axis improves non-alcoholic fatty liver disease through activation of autophagy. Sci Rep *6*, 35732.

Kmoch, S., Majewski, J., Ramamurthy, V., Cao, S., Fahiminiya, S., Ren, H., MacDonald, I.M., Lopez, I., Sun, V., Keser, V.*, et al.* (2015). Mutations in *PNPLA6* are linked to photoreceptor degeneration and various forms of childhood blindness. Nat Commun *6*, 5614.

Komninou, D., Leutzinger, Y., Reddy, B.S., and Richie, J.P., Jr. (2006). Methionine restriction inhibits colon carcinogenesis. Nutr Cancer *54*, 202-208.

Larrodera, P., Cornet, M.E., Diaz-Meco, M.T., Lopez-Barahona, M., Diaz-Laviada, I., Guddal, P.H., Johansen, T., and Moscat, J. (1990). Phospholipase C-mediated hydrolysis of phosphatidylcholine is an important step in PDGF-stimulated DNA synthesis. Cell *61*, 1113-1120.

Law, S.H., Chan, M.L., Marathe, G.K., Parveen, F., Chen, C.H., and Ke, L.Y. (2019). An updated review of lysophosphatidylcholine metabolism in human diseases. Int J Mol Sci *20*.

Lee, S., Uchida, Y., Emoto, K., Umeda, M., Kuge, O., Taguchi, T., and Arai, H. (2012). Impaired retrograde membrane traffic through endosomes in a mutant CHO cell defective in phosphatidylserine synthesis. Genes Cells *17*, 728-736.

Li, Y., and Tollefsbol, T.O. (2010). Impact on DNA methylation in cancer prevention and therapy by bioactive dietary components. Curr Med Chem *17*, 2141-2151.

Li, Y.N., Gulati, S., Baker, P.J., Brody, L.C., Banerjee, R., and Kruger, W.D. (1996). Cloning, mapping and RNA analysis of the human methionine synthase gene. Hum Mol Genet *5*, 1851-1858.

Li, Z., Agellon, L.B., Allen, T.M., Umeda, M., Jewell, L., Mason, A., and Vance, D.E. (2006). The ratio of phosphatidylcholine to phosphatidylethanolamine influences membrane integrity and steatohepatitis. Cell Metab *3*, 321-331.

Li, Z., Agellon, L.B., and Vance, D.E. (2005). Phosphatidylcholine homeostasis and liver failure. J Biol Chem *280*, 37798-37802.

Li, Z., and Vance, D.E. (2008). Phosphatidylcholine and choline homeostasis. J Lipid Res *49*, 1187-1194.

Lozano-Rosas, M.G., Chavez, E., Velasco-Loyden, G., Dominguez-Lopez, M., Martinez-Perez, L., and Chagoya De Sanchez, V. (2020). Diminished S-adenosylmethionine biosynthesis and its metabolism in a model of hepatocellular carcinoma is recuperated by an adenosine derivative. Cancer Biol Ther *21*, 81-94.

Lu, S.C., Alvarez, L., Huang, Z.Z., Chen, L., An, W., Corrales, F.J., Avila, M.A., Kanel, G., and Mato, J.M. (2001). Methionine adenosyltransferase 1A knockout mice are predisposed to liver injury and exhibit increased expression of genes involved in proliferation. Proc Natl Acad Sci U S A *98*, 5560-5565.

Lu, S.C., and Mato, J.M. (2012). *S*-adenosylmethionine in liver health, injury, and cancer. Physiol Rev *92*, 1515-1542.

Luka, Z., Mudd, S.H., and Wagner, C. (2009). Glycine *N*-methyltransferase and regulation of *S*-adenosylmethionine levels. J Biol Chem *284*, 22507-22511.

Maddocks, O.D., Labuschagne, C.F., Adams, P.D., and Vousden, K.H. (2016). Serine metabolism supports the methionine cycle and DNA/RNA methylation through de novo ATP synthesis in cancer cells. Mol Cell *61*, 210-221.

Malloy, V.L., Perrone, C.E., Mattocks, D.A., Ables, G.P., Caliendo, N.S., Orentreich, D.S., and Orentreich, N. (2013). Methionine restriction prevents the progression of hepatic steatosis in leptin-deficient obese mice. Metabolism *62*, 1651-1661.

Martin, A., Saqib, K.M., Hodgkin, M.N., Brown, F.D., Pettit, T.R., Armstrong, S., and Wakelam, M.J. (1997). Role and regulation of phospholipase D signalling. Biochem Soc Trans *25*, 1157-1160.

Martinez-Chantar, M.L., Corrales, F.J., Martinez-Cruz, L.A., Garcia-Trevijano, E.R., Huang, Z.Z., Chen, L., Kanel, G., Avila, M.A., Mato, J.M., and Lu, S.C. (2002). Spontaneous oxidative stress and liver tumors in mice lacking methionine adenosyltransferase 1A. FASEB J *16*, 1292-1294.

Mato, J.M., Corrales, F.J., Lu, S.C., and Avila, M.A. (2002). S-Adenosylmethionine: a control switch that regulates liver function. FASEB J *16*, 15-26.

Matsumoto, M., Pocai, A., Rossetti, L., Depinho, R.A., and Accili, D. (2007). Impaired regulation of hepatic glucose production in mice lacking the forkhead transcription factor Foxo1 in liver. Cell Metab *6*, 208-216.

Matsumura, H., Hasuwa, H., Inoue, N., Ikawa, M., and Okabe, M. (2004). Lineage-specific cell disruption in living mice by Cre-mediated expression of diphtheria toxin A chain. Biochem Biophys Res Commun *321*, 275-279.

McBreairty, L.E., and Bertolo, R.F. (2016). The dynamics of methionine supply and demand

during early development. Appl Physiol Nutr Metab *41*, 581-587.

Mentch, S.J., and Locasale, J.W. (2016). One-carbon metabolism and epigenetics: understanding the specificity. Ann N Y Acad Sci *1363*, 91-98.

Mittelstrass, K., and Waldenberger, M. (2018). DNA methylation in human lipid metabolism and related diseases. Curr Opin Lipidol *29*, 116-124.

Moghe, A., Joshi-Barve, S., Ghare, S., Gobejishvili, L., Kirpich, I., McClain, C.J., and Barve, S. (2011). Histone modifications and alcohol-induced liver disease: are altered nutrients the missing link? World J Gastroenterol *17*, 2465-2472.

Mohamed, J.S., Lopez, M.A., Cox, G.A., and Boriek, A.M. (2013). Ankyrin repeat domain protein 2 and inhibitor of DNA binding 3 cooperatively inhibit myoblast differentiation by physical interaction. J Biol Chem *288*, 24560-24568.

Morgan, N.V., Westaway, S.K., Morton, J.E., Gregory, A., Gissen, P., Sonek, S., Cangul, H., Coryell, J., Canham, N., Nardocci, N.*, et al.* (2006). *PLA2G6*, encoding a phospholipase A_2, is mutated in neurodegenerative disorders with high brain iron. Nat Genet *38*, 752-754.

Murakami, M. (2017). Lipoquality control by phospholipase A_2 enzymes. Proc Jpn Acad Ser B Phys Biol Sci *93*, 677-702.

Murakami, M., Taketomi, Y., Miki, Y., Sato, H., Hirabayashi, T., and Yamamoto, K. (2011). Recent progress in phospholipase A_2 research: from cells to animals to humans. Prog Lipid Res *50*, 152-192.

Ogawa, T., Tsubakiyama, R., Kanai, M., Koyama, T., Fujii, T., Iefuji, H., Soga, T., Kume, K., Miyakawa, T., Hirata, D.*, et al.* (2016). Stimulating *S*-adenosyl-L-methionine synthesis extends lifespan via activation of AMPK. Proc Natl Acad Sci U S A *113*, 11913-11918.

Parkhitko, A.A., Jouandin, P., Mohr, S.E., and Perrimon, N. (2019). Methionine metabolism and methyltransferases in the regulation of aging and lifespan extension across species. Aging Cell *18*, e13034.

Pascale, R.M., Feo, C.F., Calvisi, D.F., and Feo, F. (2018). Deregulation of methionine metabolism as determinant of progression and prognosis of hepatocellular carcinoma. Transl Gastroenterol Hepatol *3*, 36.

Pascale, R.M., Marras, V., Simile, M.M., Daino, L., Pinna, G., Bennati, S., Carta, M., Seddaiu, M.A., Massarelli, G., and Feo, F. (1992). Chemoprevention of rat liver carcinogenesis by *S*-adenosyl-L-methionine: a long-term study. Cancer Res *52*, 4979-4986.

Ramani, K., and Lu, S.C. (2017). Methionine adenosyltransferases in liver health and diseases. Liver Res *1*, 103-111.

Reytor, E., Perez-Miguelsanz, J., Alvarez, L., Perez-Sala, D., and Pajares, M.A. (2009). Conformational signals in the C-terminal domain of methionine adenosyltransferase I/III determine its nucleocytoplasmic distribution. FASEB J *23*, 3347-3360.

Robinson, J.L., McBreairty, L.E., Randell, E.W., Brunton, J.A., and Bertolo, R.F. (2016). Restriction of dietary methyl donors limits methionine availability and affects the partitioning

of dietary methionine for creatine and phosphatidylcholine synthesis in the neonatal piglet. J Nutr Biochem *35*, 81-86.

Romeo, S., Kozlitina, J., Xing, C., Pertsemlidis, A., Cox, D., Pennacchio, L.A., Boerwinkle, E., Cohen, J.C., and Hobbs, H.H. (2008). Genetic variation in *PNPLA3* confers susceptibility to nonalcoholic fatty liver disease. Nat Genet *40*, 1461-1465.

Salati, L.M., Goodridge, A.G. (1996). Fatty acid synthesis in eukaryotes. In Biochemistry of Lipids, Lipoproteins and membranes, Dennis Vance, J.E. Vance ed. (Amsterdam, Netherlands: Elsevier Science), pp. 101-128.

Sakurai, Y., Kubota, N., Takamoto, I., Obata, A., Iwamoto, M., Hayashi, T., Aihara, M., Kubota, T., Nishihara, H., and Kadowaki, T. (2017). Role of insulin receptor substrates in the progression of hepatocellular carcinoma. Sci Rep *7*, 5387.

Salgado-Albarran, M., Gonzalez-Barrios, R., Guerra-Calderas, L., Alcaraz, N., Estefania Sanchez-Correa, T., Castro-Hernandez, C., Sanchez-Perez, Y., Arechaga-Ocampo, E., Garcia-Carranca, A., Cantu de Leon, D.*, et al.* (2019). The epigenetic factor BORIS (CTCFL) controls the androgen receptor regulatory network in ovarian cancer. Oncogenesis *8*, 41.

Sanderson, S.M., Gao, X., Dai, Z., and Locasale, J.W. (2019). Methionine metabolism in health and cancer: a nexus of diet and precision medicine. Nat Rev Cancer *19*, 625-637.

Satoh, K., Yachida, S., Sugimoto, M., Oshima, M., Nakagawa, T., Akamoto, S., Tabata, S., Saitoh, K., Kato, K., Sato, S.*, et al.* (2017). Global metabolic reprogramming of colorectal

cancer occurs at adenoma stage and is induced by MYC. Proc Natl Acad Sci U S A *114*, E7697-E7706.

Saunders, C.J., Moon, S.H., Liu, X., Thiffault, I., Coffman, K., LePichon, J.B., Taboada, E., Smith, L.D., Farrow, E.G., Miller, N.*, et al.* (2015). Loss of function variants in human PNPLA8 encoding calcium-independent phospholipase $A_2\gamma$ recapitulate the mitochondriopathy of the homologous null mouse. Human mutation *36*, 301-306.

Sauter, M., Moffatt, B., Saechao, M.C., Hell, R., and Wirtz, M. (2013). Methionine salvage and *S*-adenosylmethionine: essential links between sulfur, ethylene and polyamine biosynthesis. Biochem J *451*, 145-154.

Shindou, H., and Shimizu, T. (2009). Acyl-CoA:lysophospholipid acyltransferases. J Biol Chem *284*, 1-5.

Sinha, R., Cooper, T.K., Rogers, C.J., Sinha, I., Turbitt, W.J., Calcagnotto, A., Perrone, C.E., and Richie, J.P., Jr. (2014). Dietary methionine restriction inhibits prostatic intraepithelial neoplasia in TRAMP mice. Prostate *74*, 1663-1673.

Snell, K., Natsumeda, Y., and Weber, G. (1987). The modulation of serine metabolism in hepatoma 3924A during different phases of cellular proliferation in culture. Biochem J *245*, 609-612.

Sreekumar, A., Poisson, L.M., Rajendiran, T.M., Khan, A.P., Cao, Q., Yu, J., Laxman, B., Mehra, R., Lonigro, R.J., Li, Y.*, et al.* (2009). Metabolomic profiles delineate potential role for

sarcosine in prostate cancer progression. Nature *457*, 910-914.

Stoyanov, E., Mizrahi, L., Olam, D., Schnitzer-Perlman, T., Galun, E., and Goldenberg, D.S. (2017). Tumor-suppressive effect of S-adenosylmethionine supplementation in a murine model of inflammation-mediated hepatocarcinogenesis is dependent on treatment longevity. Oncotarget *8*, 104772-104784.

Teng, Y.W., Ellis, J.M., Coleman, R.A., and Zeisel, S.H. (2012). Mouse betaine-homocysteine *S*-methyltransferase deficiency reduces body fat via increasing energy expenditure and impairing lipid synthesis and enhancing glucose oxidation in white adipose tissue. J Biol Chem *287*, 16187-16198.

Tomasi, M.L., Ramani, K., Lopitz-Otsoa, F., Rodriguez, M.S., Li, T.W., Ko, K., Yang, H., Bardag-Gorce, F., Iglesias-Ara, A., Feo, F.*, et al.* (2010). *S*-adenosylmethionine regulates dual-specificity mitogen-activated protein kinase phosphatase expression in mouse and human hepatocytes. Hepatology *51*, 2152-2161.

van der Veen, J.N., Kennelly, J.P., Wan, S., Vance, J.E., Vance, D.E., and Jacobs, R.L. (2017). The critical role of phosphatidylcholine and phosphatidylethanolamine metabolism in health and disease. Biochim Biophys Acta Biomembr *1859*, 1558-1572.

Vance, D.E. (2013). Physiological roles of phosphatidylethanolamine *N*-methyltransferase. Biochim Biophys Acta *1831*, 626-632.

Wang, C., Ruan, P., Zhao, Y., Li, X., Wang, J., Wu, X., Liu, T., Wang, S., Hou, J., Li, W.*, et al.*

(2017a). Spermidine/spermine N^1-acetyltransferase regulates cell growth and metastasis *via* AKT/β-catenin signaling pathways in hepatocellular and colorectal carcinoma cells. Oncotarget *8*, 1092-1109.

Wang, Y., Sun, Z., and Szyf, M. (2017b). S-adenosyl-methionine (SAM) alters the transcriptome and methylome and specifically blocks growth and invasiveness of liver cancer cells. Oncotarget *8*, 111866-111881.

Wang, Z., Yip, L.Y., Lee, J.H.J., Wu, Z., Chew, H.Y., Chong, P.K.W., Teo, C.C., Ang, H.Y., Peh, K.L.E., Yuan, J.*, et al.* (2019). Methionine is a metabolic dependency of tumor-initiating cells. Nat Med *25*, 825-837.

Weng, X., Wu, J., Lv, Z., Peng, C., Chen, J., Zhang, C., He, B., Tong, R., Hu, W., Ding, C.*, et al.* (2019). Targeting Mybbp1a suppresses HCC progression via inhibiting IGF1/AKT pathway by CpG islands hypo-methylation dependent promotion of IGFBP5. EBioMedicine *44*, 225-236.

Xu, S., Xu, Y., Yin, M., Zhang, S., Liu, P., Koroleva, M., Si, S., Little, P.J., Pelisek, J., and Jin, Z.G. (2018). Flow-dependent epigenetic regulation of IGFBP5 expression by H3K27me3 contributes to endothelial anti-inflammatory effects. Theranostics *8*, 3007-3021.

Yanaka, N. (2007). Mammalian glycerophosphodiester phosphodiesterases. Biosci Biotechnol Biochem *71*, 1811-1818.

Ye, C., Sutter, B.M., Wang, Y., Kuang, Z., and Tu, B.P. (2017). A metabolic function for

phospholipid and histone methylation. Mol Cell *66*, 180-193 e188.

Zabala-Letona, A., Arruabarrena-Aristorena, A., Martin-Martin, N., Fernandez-Ruiz, S., Sutherland, J.D., Clasquin, M., Tomas-Cortazar, J., Jimenez, J., Torres, I., Quang, P.*, et al.* (2017). mTORC1-dependent AMD1 regulation sustains polyamine metabolism in prostate cancer. Nature *547*, 109-113.

Zeisel, S.H., and da Costa, K.A. (2009). Choline: an essential nutrient for public health. Nutr Rev *67*, 615-623.

Zhang, X., Zhang, J., Wang, R., Guo, S., Zhang, H., Ma, Y., Liu, Q., Chu, H., Xu, X., Zhang, Y.*, et al.* (2016). Hypermethylation reduces the expression of PNPLA7 in hepatocellular carcinoma. Oncol Lett *12*, 670-674.

Zheng, Y., and Cantley, L.C. (2019). Toward a better understanding of folate metabolism in health and disease. J Exp Med *216*, 253-266.

Zheng, Y., Thomas, P.M., and Kelleher, N.L. (2013). Measurement of acetylation turnover at distinct lysines in human histones identifies long-lived acetylation sites. Nat Commun *4*, 2203.

Zhong, J., Agha, G., and Baccarelli, A.A. (2016). The Role of DNA Methylation in Cardiovascular Risk and Disease: Methodological Aspects, Study Design, and Data Analysis for Epidemiological Studies. Circ Res *118*, 119-131.

Zhou, X., He, L., Wan, D., Yang, H., Yao, K., Wu, G., Wu, X., and Yin, Y. (2016). Methionine restriction on lipid metabolism and its possible mechanisms. Amino Acids *48*, 1533-1540.

Zhu, J., Berisa, M., Schworer, S., Qin, W., Cross, J.R., and Thompson, C.B. (2019). Transsulfuration activity can support cell growth upon extracellular cysteine limitation. Cell Metab *30*, 865-876 e865.

Acknowledgment

I would like to express my sincere gratitude to my advisor Prof. Makoto Murakami for the continuous support of my Ph.D. research, helpful discussions and knowledge, and his heart to value my interests. I joined his team at my second year, I profoundly appreciate for welcoming me to his team.

I would like to express my sincere gratitude to assistant professor Dr. Yoshitaka Taketomi for encouraging me and tremendous support for me. He always helped me a lot throughout my research.

I would like to express my sincere gratitude to associate professor Dr. Seiichiro Ohsako for helpful comments and suggestions. Because I had been worked under his instruction for my first year, I am extremely grateful for welcoming me to his laboratory.

I would like to acknowledge with much appreciation to Dr. Tomoyoshi Soga and his research members (Institute for Advanced Biosciences, Keio University) for giving me the valuable metabolome data. My research could not have been completed without their support.

I would also like to acknowledge with much appreciation to Dr. Yutaka Yatomi and his research members (the Department of Laboratory Medicine, the University of Tokyo) for providing

clinical samples. My research was blossomed with the analysis of these samples and could not have been completed without them.

I would like to express my special thank to Dr. Toshiki Aiba (National Institutes for Quantum and Radiological Science and Technology). He has motivated me, mentored me, and supported me throughout my research for 4 years. Furthermore, my research could not have completed without his support.

I would also like to thank to Dr. Tetsuya Hirabayashi and Mai Kawaguchi (PhD. student) for your cooperation about mouse liver.

I would also like to express my special thank to Dr. Eiki Kimura (University of Cincinnati) for his helpful and valuable advices.

My deepest appreciation to my seniors, Dr. Hiroyasu Sato, Dr. Yoshimi Miki, Dr. Naota Kuwahara, Takayoshi Higashi (Ph.D. student) and all other lab members and collaborators for their technical instructions and supports, and encouragements for me.

Beside my research, I would also my deepest and special thanks to my family and friends, especially for Dr. Ippei Harada, who supported me financially and mentally and consulted me all the time, for K. T. and H. T., who entertained me all the time, and for H. I., who motivated and encouraged me a lot all the time.